

25 **Abstract**

26 The vancomycin-resistant *Enterococcus faecalis* alkyl hydroperoxide reductase complex
27 (AhpR) with its subunits AhpC (*EfAhpC*) and AhpF (*EfAhpF*) is of paramount importance to
28 restore redox homeostasis. Therefore, knowledge about this defense system is essential to
29 understand its antibiotic-resistance and survival in hosts. Recently, we described the
30 crystallographic structures of *EfAhpC*, the two-fold thioredoxin-like domain of *EfAhpF*, the
31 novel phenomenon of swapping of the catalytic domains of *EfAhpF* as well as the unique
32 linker length, connecting the catalytically active N-and C-terminal domains of *EfAhpF*. Here,
33 using mutagenesis and enzymatic studies, we reveal the effect of an additional third cysteine
34 (C503) in *EfAhpF*, which might optimize the functional adaptation of the *E. faecalis* enzyme
35 under various physiological conditions. The crystal structure and solution NMR data of the
36 engineered C503A mutant of the thioredoxin-like domain of *EfAhpF* were used to describe
37 alterations in the environment of the additional cysteine residue during modulation of the
38 redox-state. To glean insight into the epitope and mechanism of *EfAhpF* and -AhpC
39 interaction as well as the electron transfer from the thioredoxin-like domain of *EfAhpF* to
40 AhpC, NMR-titration experiments were performed, showing a coordinated disappearance of
41 peaks in the thioredoxin-like domain of *EfAhpF* in the presence of full length *EfAhpC*, and
42 indicating a stable *EfAhpF*-AhpC-complex. Combined with docking studies, the interacting
43 residues of *EfAhpF* were identified and a mechanism of electron transfer of the *EfAhpC*
44 donor to the electron acceptor *EfAhpF* is described.

45 1. Introduction

46 *Enterococcus faecalis* is a ubiquitous and opportunistic gram-positive microorganism
47 responsible for 90% of nosocomial infections [1]. Compounding the pathogenicity of *E.*
48 *faecalis* is its rapid development of resistance towards antimicrobial agents, the most
49 common being the Vancomycin-Resistant Enterococcus (VRE) [2-3]. *E. faecalis* has evolved
50 numerous virulence factors that ensure its survivability under harsh conditions of including
51 reactive oxygen species (ROS) such as hydrogen peroxide (H₂O₂) inside macrophages [2,3].
52 The ability of *E. faecalis* to survive the intolerant ROS condition of the macrophage implies
53 the presence of robust antioxidant systems [4] to which the Alkyl hydroperoxide reductase
54 complex (AhpR) does belong too, which may serve as therapeutic targets for the prevention
55 of early stages of infections [5, 6].

56 The *E. faecalis* AhpR system is driven by two proteins, a 2-Cys peroxiredoxin, AhpC
57 (*EfAhpC*) and a thiol-dependent peroxiredoxin reductase, AhpF (*EfAhpF*) to catalyse the
58 NADH-dependent reduction of hydrogen peroxide [4] (Fig. 1A). The catalytic centre of
59 AhpC is composed of two active cysteine residues; peroxidatic (C_P) and reducing (C_R). The
60 peroxidatic cysteine residue (C_P) of one subunit of AhpC first reacts with a molecule of
61 hydrogen peroxide to form sulfenic acid. Then a reducing cysteine residue (C_R) of the
62 adjacent unit of AhpC attacks the sulfenic acid bond, producing water molecule and oxidised
63 AhpC [4, 7]. As demonstrated by EM-data and the crystallographic structure, *EfAhpC* forms
64 a decamer independent to the redox state [7] (Fig. 1A). This is unlike AhpCs of gram-
65 negative bacteria like *Escherichia coli* (*EcAhpC*) and *Staphylococcus aureus* (*StAhpC*),
66 which form a stable decamer in the reduced form and lower weight oligomers in the oxidized
67 state [8-10]. In comparison, besides the two typical catalytic cysteine residues C_P and C_R,
68 *EfAhpC* has two additional cysteines, with C13 and C66 at the N-terminus, which are
69 important for stabilization of the decameric ring and enzyme activity [7].

70 Oxidised AhpC is regenerated via the reducing action of AhpF [11]. The latter is a
71 homodimeric protein which is composed of two domains with a flexible linker in-between
72 [12, 13]. The electron donor NADH first docks at its binding site located at the pyridine
73 nucleotide-disulfide oxidoreductase domain (CTD:Pyr_redox_2). This sets off cascading
74 steps of electron transfer from the NADH molecule via FAD (flavin adenine dinucleotide), a
75 prosthetic group to the first CXXC-motif located at the same domain. The second CXXC-
76 motif residing at the two-fold thioredoxin-like domain (NTD_N/C) will then come close to
77 the first reduced CXXC-motif and pick up the electron. This allows the reduced second
78 CXXC-motif to regenerate the reducing potential of oxidised AhpCs [11, 13, 14].

79 We had first described the unique phenomenon of AhpF protein in *E. faecalis* (V583)
80 bacteria (*EfAhpF*), highlighting the distinct structural features such as domain swapping, and
81 the unusual long flexible linker connecting the catalytic NTD_N/C and CTD:Pyr_redox_2
82 domains [13]. Our recent crystallographic structure of the *EfAhpF* NTD_N/C part unravelled
83 a unique loop-helix stretch (₄₀₉ILKDTEPAKELLYGIEKM₄₂₆) not present in homologue
84 domains of other prokaryotic AhpFs. Deletion of the ₄₁₅PAKELLY₄₂₁-helix affected protein
85 stability or attenuates peroxidase activity [13].

86 Besides the significant differences of *EfAhpF* compared to its counterpart in other AhpFs
87 described above, *EfAhpF* harbours one additional cysteine, C503, in the NTD_N/C domain.
88 In analogy to the two additional cysteines (C13, C66) of *EfAhpC*, relevant for stabilization of
89 the decameric ring and enzyme activity [7], we sought to investigate the significance of C503
90 of *EfAhpF* using a complementary approach of mutagenesis, enzyme assays, crystallography,
91 and NMR solution spectroscopy. In addition, the complex formation of *EfAhpF*-AhpC is
92 closely studied here using NMR analysis. Coupled with our previous published results, these
93 data will lead to a better understanding of the *E. faecalis* (V583) AhpR system in *E. faecalis*
94 (V583) which can then be exploited as a therapeutic target.

95 2. Materials and Methods

96 2.1 Cloning of *EfAhpF*, *AhpC* and their mutants

97 Wild type (WT) *EfAhpF* and *EfAhpF*₃₅₄₋₅₆₀ were cloned into the pET9-d1-His6 vector
98 [15] as described in the paper [13]. Cloning of *EfAhpC* and its single mutants C13N and
99 C66V as well as double mutant C13N/C66V was performed as described recently by Pan et
100 al. [7]. Full-length *EfAhpF* C503A and *EfAhpF*₃₅₄₋₅₆₀ C503A were cloned with forward
101 primer (5' – GTCGTGGCGGCTGCCCAACGTATT – 3') (underlined indicates single amino
102 acid substitution) and reverse primer (5' –
103 ATCGGGACAGAAATGACATGTTAGTGAAACAAAGATTTC – 3'), using respective
104 wild-type *EfAhpF* vector as template by non-overlapping site-directed mutagenesis. The PCR
105 products were *DpnI*-digested before purified and transformed into *E. coli* DH5 α cells.

106

107 2.2 Purification of WT and mutant proteins of *E. faecalis*

108 WT *E. faecalis* AhpR subunits AhpC and F as well as their mutants were transformed into
109 *E. coli* BL21 (DE3) cells (Stratagene, USA) and induced with 1 mM isopropyl β -D-1-
110 thiogalactopyranoside (IPTG) at 20 °C (*EfAhpF*) or 37 °C (*EfAhpC*) for protein production.
111 Cells were lysed on ice by sonication for 3 \times 1 min in buffer A (50 mM Tris/HCl, pH 7.5,
112 200 mM NaCl, 0.8 mM DTT and 2 mM Pefabloc^{SC} (BIOMOL)). The cell lysate was
113 centrifuged at 10 000 \times g for 35 min before the supernatant was filtered (0.45 μ m; Millipore)
114 and incubated with Ni-NTA Agarose (Qiagen) for one hour at 4 °C. His₆-tagged protein was
115 then eluted with an imidazole gradient (20 mM to 500 mM) in Buffer A. For *EfAhpC*, pooled
116 fractions containing the protein of interest were applied onto a gel filtration column
117 (SuperdexTM 200 HR 10/300 column, GE Healthcare) in buffer B (50 mM Tris/HCl, pH 7.5
118 and 200 mM NaCl). In the case of *EfAhpF*, fractions containing the recombinant protein were
119 pooled and applied onto an anion chromatography column ResourceQ (6 ml). Fractions

120 containing recombinant protein were pooled and applied onto a gel filtration column
121 (Superdex™ 200 HR 10/300 column, GE Healthcare) in buffer B (50 mM Tris/HCl, pH 7.5
122 and 200 mM NaCl), and the purified recombinant protein was pooled and concentrated. All
123 other *EfAhpF* mutants were purified according to the WT *EfAhpF* purification protocol [13].

124

125 **2.3 Crystallization of *EfAhpF*₃₅₄₋₅₆₀ C503A**

126 Recombinant *EfAhpF*₃₅₄₋₅₆₀ (NTD_N/C) C503A mutant was concentrated to 5 mg/ml in a
127 buffer composed of 50 mM Tris/HCl, pH 7.5 and 200 mM NaCl. Hexagonal-shaped crystals
128 were grown in precipitant solution of 0.1 M Bis-Tris (pH 6.5), 1.5 M ammonium sulfate and
129 0.1 M sodium chloride by hanging-drop vapor-diffusion method. The final *EfAhpF*₃₅₄₋₅₆₀
130 C503A crystals were flash-frozen in liquid nitrogen at 100 K in crystallization buffer
131 containing 0.1 M Bis-Tris (pH 6.5), 2.0 M ammonium sulfate, 0.1 M sodium chloride and 2.0
132 M Proline.

133

134 **2.4 Data collection and structure determination of *EfAhpF*₃₅₄₋₅₆₀ C503A**

135 X-ray diffraction data for the *EfAhpF*₃₅₄₋₅₆₀ C503A were collected at 100 K at beamline
136 13B1 of the National Synchrotron Radiation Research Centre (NSRRC, Hsinchu, Taiwan)
137 using the ADSC Quantum 315 CCD detector. Data were collected as a series of 0.5°
138 oscillation images covering a crystal rotation range of 100° on cryo-cooled crystals. A
139 complete 2.5 Å data set was collected and the diffraction data were indexed, integrated and
140 scaled using HKL2000 suite [16]. The results of data processing and data statistics are
141 summarized in Table 1. The crystallographic structure was solved by molecular replacement
142 method using WT *EfAhpF*₃₅₄₋₅₆₀ structure (PDB ID: 5H29) [13] as model in PHASER [17].
143 The starting model was improved by iterative cycles of model building manually using Coot
144 [18] and refinement by REFMAC5 [19] of CCP4 suite. Refinement was done until

145 convergence and the geometry of the final model was validated with MolProbity [20]. This
146 analysis indicated that the overall geometry of the final model ranked in the 100th percentile
147 (MolProbity score of 1.23). The clash score for all atoms was 1.22 corresponding to a 100th
148 percentile ranking of structures of comparable resolution. The data were cut off at 2.5 Å
149 based on the $CC_{1/2}$ statistics [20] (correlation coefficient between two random halves of the
150 data set where $CC_{1/2} > 10\%$) to determine the high-resolution cut-off for our data. Phenix [21]
151 was used to compute $CC_{1/2}$ (97.5% for the highest resolution shell and 99.9% for the entire
152 data set), supporting our high-resolution cut-off determination. The figures were drawn using
153 PyMOL [22] and structural comparison analysis was carried out using SUPERPOSE [23]
154 from CCP4 suite [24, 25]. The coordinates and structure factors of *EfAhpF*₃₅₄₋₅₆₀ C503A at 2.5
155 Å have been deposited in the Protein Data Bank with accession code [6IL7].

156

157 **2.5 NADH-dependent peroxidase assay**

158 NADH-dependent peroxidase assay was monitored at 340 nm following the decrease in
159 NADH absorbance using a stopped flow spectrophotometer Applied Photophysics SX20. The
160 assay was carried out at 25 °C containing a 100 mM phosphate buffer at pH 7.0, 200 mM
161 ammonium sulfate and 1 mM EDTA. One syringe arm contained a final concentration of 200
162 μM of NADH, 100 μM of H₂O₂, increasing concentration of AhpC [1 - 80 μM], and the other
163 arm contained a final concentration of 100 nM WT *EfAhpF* or *EfAhpF* C503A mutant. The
164 assay was done in triplicates. Michaelis-Menten plots were created using program Origin Pro
165 9.0 (OriginLab Corporation).

166

167 **2.6 Ferrous oxidation xylenol orange (FOX) assay**

168 Hydrogen peroxide reduction catalysed by *EfAhpC* in the presence of *EfAhpF* was
169 measured in PeroxiDetect™ kit by Sigma-Aldrich®. The kit is based on the principle of

170 ferrous oxidation xylenol orange assay. 100 μ l of reaction mixture containing 50 mM HEPES
171 buffer pH 7.0, 100 μ M H₂O₂, 250 μ M NADH, 15 μ M WT *EfAhpC* or *EfAhpC* mutants and
172 0.4 μ M WT *EfAhpF* or *EfAhpF* C503A were prepared from which 10 μ l of aliquots were
173 removed at specific time intervals and added to 190 μ l of FOX reagent before incubating for
174 at least 30 mins at room temperature. The absorbance of the sample was then measured at $\lambda =$
175 560 nm for detection of H₂O₂.

176

177 **2.7 NMR analysis of *EfAhpF*₃₅₄₋₅₆₀**

178 0.7 mM of ¹⁵N/¹³C double-labelled *EfAhpF*₃₁₄₋₅₆₀ was prepared in 50 mM sodium
179 phosphate pH 6.8, 50 mM NaCl, 10% D₂O in the presence or absence of 2 mM TCEP (tris(2-
180 carboxyethyl)phosphine) according to the purification method described above. NMR
181 measurements were performed on 700 MHz Bruker Avance NMR spectrometer equipped
182 with 5 mm triple-resonance (¹H/¹⁵N/¹³C) single axis gradient cryogenic probes at 298K.

183 To assign the backbone of *EfAhpF*₃₅₄₋₅₆₀, both uniform (traditional) and non-uniform
184 sampling (NUS; [26]) techniques were employed to acquire the data. 2D-¹H-¹⁵N TROSY-
185 HSQC data were collected with conventional linear sampling technique, whereas all triple
186 resonance experiments, including TROSY-HNCACB, 3D-TROSY-HN(CO)CACB,
187 CBCA(CO)NH, HNCA and HN(CO)CA data were collected using NUS techniques of the
188 indirect dimension as 20% sampling rates and reconstructed using compressed sensing (CS)
189 scheme using MDDNMR software [27,28]. All NMR-spectra were processed using
190 NMRpipe [29] and analyzed with SPARKY program [30]. Both techniques enabled the
191 assignment of 90% of the backbone resonances (N, CA, HN).

192 Titration of 0.3 mM uniformly ¹⁵N-labelled *EfAhpF*₃₅₄₋₅₆₀ or *EfAhpF*-C503A₃₅₄₋₅₆₀ with
193 oxidized *EfAhpC* was performed to achieve incremental molar equivalents of 0.05 and 0.1.
194 ¹H-¹⁵N TROSY-HSQC spectra were recorded with 2,048 complex data points in t_2 and 256

195 t_1 increments at molar ratios of 1 (*EfAhpF*) : 0 (*EfAhpC*), 1:0.05 and 1:0.1, respectively.
196 Spectral width of 2,270 and 11,160 Hz were employed in F1(¹⁵N) and F2(¹H), respectively.
197 The combined chemical shift perturbation, the peak intensity and line width informations
198 were extracted to determine molecular interaction between two proteins.

199

200 **2.8 High Ambiguity Driven DOCKing(HADDOCK) modeling of *EfAhpF*₃₅₄₋₅₆₀ and** 201 ***EfAhpC*₁₋₁₆₇**

202 Experimentally identified binding interfacial residues of *EfAhpF*₃₅₄₋₅₆₀, excluding the extra
203 flexible loop from amino acids A314-Q353, were used to perform docking studies, and to
204 model the complex of *EfAhpF*₃₅₄₋₅₆₀ and *EfAhpC*₁₋₁₆₇ using the HADDOCK webserver [31].
205 The experimentally determined crystal structures for the *EfAhpF*₃₅₄₋₅₆₀ and *EfAhpC*₁₋₁₆₇ dimer
206 were used for docking simulation. Surface exposed residues experiencing intensity and
207 linewidth changes during titration were used as restraints. Since HADDOCK requires a set of
208 ambiguous interaction restraints, residues directly interacting at the interface need to be
209 specified as “active” residues and neighbouring residues as “passive”. The experimentally
210 obtained interacting residues were set as active. In the case of *EfAhpC*₁₋₁₆₇, a dimeric unit of
211 coordinates from the crystal structure were submitted to the meta-PPISP for protein–protein
212 interfacial residues prediction [32]. These predicted interfacial residues were set as “active”
213 residues. These restraints were used as input for the HADDOCK webserver and default
214 parameters were used for docking. The resulting structures were clustered by a cut-off value
215 (7.5 Å). Finally, based on the HADDOCK score and total energy, the best model from the
216 highest scoring cluster was selected for analysis. The model was visualized using the PyMOL
217 software [22].

218

219

220 **3. Results**

221 **3.1 Sequence analysis of *E. faecalis* AhpF's two-fold thioredoxin-like domain** 222 **(NTD_N/C)**

223 Inspection of the *EfAhpF* protein sequence showed that its two-fold thioredoxin-like
224 domain (NTD_N/C) contains an additional cysteine residue at position 503 in helix α 6 (Fig.
225 1B). To investigate whether the occurrence of this additional cysteine residue is predominant
226 in AhpFs of other species, a protein sequence alignment of AhpF NTD_N/C domains of ten
227 different species was performed. It was shown that domain swapping is a unique feature of
228 *EfAhpF* where the NTD_N/C is located at the C-terminus and the pyridine nucleotide-
229 disulfide oxidoreductase domain (CTD:Pyr_redox_2) is located at the N-terminus [13].
230 Therefore, AhpF NTD_N/C domains of five different species displaying the '*E. faecalis*-like'
231 AhpF domain localization (C-terminus) and AhpF NTD_N/C domains of another five
232 different species showing '*E. coli*-like' AhpF domain localization (N-terminus) were chosen
233 for this sequence alignment. The alignment indicates that the additional cysteine at position
234 503 is conserved across several species belonging to the '*E. faecalis*-like' subgroup, *E.*
235 *faecalis* (V583), *L. reuteri* (SD2112) and *C. stercorarium* (DSM8532), but is not present in
236 the *Bacillus* species and all sequences of the '*E. coli*-like' subgroup (Fig. 1B, red box).
237 Interestingly, both *B. bifidum* (BGN4) and *B. longum* (157F) NTD_N/C harbour two
238 additional cysteine residues in position 496 and 609 according to *B. bifidum* (BGN4)
239 numbering. To note, in all AhpF NTD_N/C domains of the species belonging to the '*E. coli*-
240 like' subgroup the cysteine residue is replaced by a leucine residue.

241

242 **3.2 Importance of the extra cysteine 503 in *EfAhpF***

243 To investigate the importance of the extra cysteine C503, this residue was mutated to
244 alanine (C503A) in the full-length *EfAhpF* construct. Kinetic studies using NADH-based

245 oxidation assay on stopped-flow spectrometer was performed (Fig. 2). WT *EfAhpF* displays a
246 k_{cat} of $46.1 \pm 4 \text{ s}^{-1}$ and a K_m (AhpC) of $24.5 \pm 5 \text{ }\mu\text{M}$, giving it an enzymatic efficiency, k_{cat}/K_m
247 (AhpC) of $1.9 \times 10^6 \text{ M}^{-1}\cdot\text{s}^{-1}$ (Fig. 2B). In contrast, the *EfAhpF* C503A mutant has a similar
248 k_{cat} of $49.2 \pm 6 \text{ s}^{-1}$ but an ~ 3 -fold higher K_m (AhpC) of $70.9 \pm 12 \text{ }\mu\text{M}$, which translates to a
249 nearly 27-fold lower catalytic efficiency of *EfAhpF* C503A where k_{cat}/K_m (AhpC) is 0.7×10^5
250 $\text{M}^{-1}\cdot\text{s}^{-1}$ (Table. 2) (Fig. 2B). The increased K_m (AhpC) of *EfAhpF* C503A suggests that the
251 mutation leads to a negative effect on its interaction with *EfAhpC*.

252 To further confirm that the C503 mutation affects the reduction of *EfAhpC*, a FOX assay
253 was performed to measure the ability of *EfAhpF* C503A together with *EfAhpC* to reduce
254 H_2O_2 (Fig. 3A). WT *EfAhpF* reduced $5 \text{ }\mu\text{M}$ of H_2O_2 in about 1 min., whereas *EfAhpF* C503A
255 reduced the same concentration of H_2O_2 in about 3 mins. This correlates with the stopped-
256 flow kinetic studies, showing that C503 is important for the catalytic activity of *EfAhpF*.

257 Our recent studies revealed, that extra cysteine residues from *EfAhpC* (C13 and C66)
258 have an important role in the *EfAhpR* system as mutation of these cysteine residues to its
259 equivalent residues in *E. coli* AhpC (C13N and C66V) adversely affected the *EfAhpR* system
260 to reduce H_2O_2 [7]. Here, *EfAhpF* C503A was analysed by the FOX assay in the presence of
261 the *EfAhpC* mutants C13N (*EfAhpC* C13N), *EfAhpC* C66V, and the double mutant *EfAhpC*
262 C13N/C66, respectively (Fig. 3B). When compared to *EfAhpC*-AhpF C503A, the mutant
263 ensemble *EfAhpC* C66V-AhpF C503A revealed a reduction in H_2O_2 decomposition which
264 became even more prominent for mutant complexes *EfAhpC* C13N-AhpF C503A followed
265 by *EfAhpC* C13N/C66-AhpF C503A, indicating an additive effect on the *EfAhpC* cysteine
266 mutants' ability to reduce H_2O_2 .

267

268

269

270 **3.3 Crystallographic structure of the *EfAhpF*₃₅₄₋₅₆₀ C503A mutant**

271 To investigate whether the substitution of C503 to alanine causes a structural change in
272 *EfAhpF* NTD_N/C, we crystallized *EfAhpF*₃₅₄₋₅₆₀ C503A in the same crystallisation solution
273 as WT *EfAhpF*₃₅₄₋₅₆₀ [13]. Crystals grew to the same cubic space group P4₁32 and the
274 determined atomic structure was refined to 2.5 Å resolution. The final R-factor and R-free
275 (calculated with 5% of reflections that were not included in the refinement) were 21.47% and
276 26.72%, respectively (Table 1). There is one molecule of *EfAhpF*₃₅₄₋₅₆₀ C503A in the
277 asymmetric unit with a solvent content of 72.06%. The *EfAhpF*₃₅₄₋₅₆₀ C503A monomer
278 contained 207 amino acid residues with almost all main chain residues fitting well into the
279 electron density. The *EfAhpF*₃₅₄₋₅₆₀ C503A monomer also contained three molecules of SO₄
280 and 67 molecules of water (Table 1). The overall structure of *EfAhpF*₃₅₄₋₅₆₀ C503A is shown
281 in figure 4A. The side chain density for all the amino acids is very well resolved. The average
282 B-factor was calculated to be 61.02 Å². Analysis of the stereo-chemical quality of the final
283 model by PROCHECK has identified that 98.1% of all the residues are within the favoured
284 regions of the Ramachandran plot, 1.9% are within the generously allowed regions. There
285 were no residues in the disallowed region.

286 When *EfAhpF*₃₅₄₋₅₆₀ C503A was overlaid with WT *EfAhpF*₃₅₄₋₅₆₀, it aligned well with an
287 r.m.s.d of 0.1 Å for 155 Cα atoms (Fig. 4B). Careful inspection of the structural
288 superimposition of both crystallographic structures did not reveal any structural alterations
289 due to the mutation of C503.

290

291 **3.4 Redox-dependent modulation within *EfAhpF*₃₅₄₋₅₆₀ C503A**

292 While the atomic structure of *EfAhpF*₃₅₄₋₅₆₀ C503A did not show a change due to the
293 mutation made, the question was addressed whether redox processes may alter the position of
294 C503 and neighbouring residues in solution. Therefore, WT *EfAhpF*₃₅₄₋₅₆₀ was studied in

295 NMR solution studies in the presence and absence of the reducing agent TCEP. As shown in
296 figure 5A, uniformly labelled *EfAhpF*₃₅₄₋₅₆₀ resulted in a well-dispersed ¹H-¹⁵N HSQC-
297 spectrum of the protein (Fig. 5), indicating proper folding and monodispersity of the
298 recombinant protein. High mobility of the linker region (A314 to Q353), which is included in
299 this construct, gave intense and sharp peaks, which in some cases overlap with other less
300 intense signals. However, this did not affect the overall quality of the spectrum. Sequential
301 backbone assignment based on the triple resonance NMR data, including HNCACB,
302 HNCOCACB, HNCA and HNCOCA enabled the assignment of ¹H and ¹⁵N resonances for
303 204 residues out of 234 non-proline residues of *EfAhpF*₃₅₄₋₅₆₀. The secondary structure
304 prediction of *EfAhpF*₃₅₄₋₅₆₀ was performed for the residues W354-A560 based on assigned
305 C α -chemical shifts, which were subtracted from their random coil values ($\Delta C\alpha$). The
306 prediction is highly consistent with the *EfAhpF*₃₅₄₋₅₆₀ crystal structure and reveals eight α -
307 helices and nine β -strands (Fig. 5B).

308 In comparison, addition of TCEP caused chemical shifts in the ¹H-¹⁵N HSQC-spectrum of
309 *EfAhpF*₃₅₄₋₅₆₀ (Supplementary Figure S1 and Fig. 5C). Based on the chemical shift
310 perturbation (CSP) analysis between reduced and oxidized *EfAhpF*₃₁₄₋₅₆₀, the residues W354,
311 S428, G445, G449, E451-N453, F488, C496, I499-C503, I506, H512, V518, V535, D541,
312 and G548 undergo significant alteration (>0.1) due to an alteration of the redox-state (Fig.
313 5D). As shown in figure 5E, the identified residues of *EfAhpF*₃₅₄₋₅₆₀ involved in redox-
314 dependent modulation form an epitope based on the neighbouring helices α 4 and α 6 as well
315 as the β -sheets 5 and 6, including C503 of helix α 6.

316

317 **3.5 NMR characterisation of a stable *EfAhpC-EfAhpF*₃₅₄₋₅₆₀ complex formation**

318 Previous studies have shown that AhpF transfers electrons to AhpC through interaction
319 with its thioredoxin-like domain (NTD_N/C) [9, 33]. To understand this interaction and

320 decipher the binding epitope, NMR titration experiments were performed, in which uniformly
321 labelled *EfAhpF*₃₅₄₋₅₆₀ was titrated against *EfAhpC*. The highly resolved and dispersed NMR-
322 spectrum of *EfAhpF*₃₅₄₋₅₆₀ mentioned above (Fig. 5A) enabled titration experiments to be
323 performed. The ¹H-¹⁵N-TROSY-HSQC spectrum was obtained for the labelled *EfAhpF*₃₅₄₋₅₆₀
324 protein alone as well as in the presence of increasing amounts of the partner protein *EfAhpC*
325 (Fig. 6A). During titration experiments, we observed the gradual disappearance or decrease
326 of overall cross peak intensities and line broadening in the ¹H-¹⁵N-TROSY-HSQC spectra
327 (Fig. 6A-B). Due to the large molecular weight of the *EfAhpF*₃₅₄₋₅₆₀-*EfAhpC* complex, the
328 majority of *EfAhpF*-NTD peaks gradually disappeared, suggesting a global decrease in
329 tumbling, consistent with a stable interaction. Since *EfAhpC* forms a decamer in solution
330 (about 210 kDa), the above mentioned observation is consistent with a stable complex.
331 However, peaks from amino acid residues in the highly flexible linker region, residues,
332 A314-Q353 showed relatively higher intensities compared with the core part of the protein
333 (W354-A560), indicating that the flexible linker region of the *EfAhpF* construct was not
334 affected by the interaction with *EfAhpC* and exhibits a local tumbling motion independent of
335 the global motion of the complex.

336

337 **3.6 Binding interface of the *EfAhpF*₃₅₄₋₅₆₀-AhpC complex**

338 To investigate the molecular interaction between *EfAhpF*₃₅₄₋₅₆₀ and *EfAhpC* in more
339 detail, NMR-titration data were analyzed in terms of the peak intensities and the line width
340 changes of the NMR spectra between *EfAhpF* and *EfAhpC* in the ratio 1:0 and 1:0.1,
341 respectively. The NMR spectra show the significant disappearances or decrease of some
342 cross peak intensities in the ¹H-¹⁵N TROSY-HSQC spectra compared with other residues
343 (Fig. 6A-B). Plots of intensity ratio (I_0/I_1) before (I_0) and after (I_1) for AhpC (I_0/I_1) and
344 increased line width for indirect ¹⁵N dimension at a molar ratio 1:0.1 are shown in the figure

345 7A-B. They reveal the candidates of the binding surface of *EfAhpF*₃₅₄₋₅₆₀ when interacting
346 with *EfAhpC*. Significant changes in intensity ratio and linewidth over standard deviation
347 were observed for the backbone resonances of residues G449-L455 (Fig. 7A), indicating that
348 these residues are considered as directly involved in the interaction with *EfAhpC*. Amino
349 acids F355, R360, Q362, F367, I444, I446, G449-L455, Q467, A502, and I506 show
350 intensity changes reflected by the standard deviation values after addition of *EfAhpC* (Fig.
351 7A). In addition, the residues including L363, E385, F397, S428, L432, I441, I446, G449-
352 L455, Q467, K475, S490, V500, E525, S534, and M552 reveal increased ¹⁵N line-widths
353 over than standard deviation (Fig. 7B).

354 Based on the NMR intensity changes and linewidth analysis data, the binding area inside
355 *EfAhpF*, which interacts with *EfAhpC*, was mapped on the crystal structure of *EfAhpF*₃₅₄₋₅₆₀
356 as shown in figure 7C, reflecting that surface exposed residues form a well-defined
357 interaction surface around the active site cysteine residue C493. Most surface exposed
358 residues (G449-L455), which show relatively high intensity changes and line width increase
359 form a clustered interaction cleft, indicating that these residues may be strongly related to
360 *EfAhpF*-*AhpC* interaction. Residues I441, I446, S448-L455, L490, T492, S521, K527, M531,
361 S532, V533, clustered closely to the catalytically active C493, might also directly participate
362 in *EfAhpF*-*AhpC* assembling. In addition, amino acids around the binding epitope such as
363 W354, F355, R360, Q362, S364, Q467 as well as S385, F396, S399, G436, T437, K401,
364 A456, V461, G476, R483, K484, E486, N510, E525, L526, M552 and E554 could be
365 indirectly related to protein-protein interaction as a result of the slight conformational
366 changes of *EfAhpF* caused by *EfAhpC*.

367

368

369

370 **3.7 The role of C503 in *EfAhpF*-AhpC interaction**

371 To shed light into the role of C503 in *EfAhpF*-AhpC interaction, NMR titration
372 experiments using mutant *EfAhpF*₃₅₄₋₅₆₀ C503A and *EfAhpC* (molar ratio 1:0.1) were
373 performed. As displayed in figures 8A-C, overall changes of decreasing intensity ratios and
374 increasing line width (¹⁵N line width) were observed. Residues G449-N453 of *EfAhpF*₃₅₄₋₅₆₀
375 C503A show relatively high intensity ratios compared to other residues, however, the relative
376 intensity changes dramatically decreased (~40%) compared to the WT protein (Fig. 7A-B),
377 indicating overall decreased interaction between *EfAhpF*₃₅₄₋₅₆₀ C503A and *EfAhpC*. In
378 addition, the residues showing changes of ¹⁵N line width within the *EfAhpF*₃₅₄₋₅₆₀ C503A
379 mutant after addition of *EfAhpC* significantly changed (Fig. 7A) when compared to WT (Fig.
380 5D), indicating that the substitution of C503A affects the interaction between *EfAhpF* and -
381 AhpC by modulation of protein conformation and dynamic properties. Moreover, ¹H-¹⁵N-
382 HSQC spectra show disappearance and significant CSPs of the resonances around C503,
383 including residues C496, A501, Q504, A507, S508, N510, H512 and E514 (Fig. 8A). These
384 observations are supporting that the C503A induce changes in conformational and dynamic
385 properties of the residues located around C503, resulting in modulation of the interaction
386 between *EfAhpF* and -AhpC. In conclusion, it is considered that C503 is not directly involved
387 in protein-protein interaction, but affects the interaction between *EfAhpF* and -AhpC by the
388 formation of a molecular interaction network with neighbouring residues.

389

390 **3.8 NMR based Docking studies of an *EfAhpF*-AhpC complex**

391 To investigate the complex formation of *EfAhpF*-AhpC, the obtained restraints based on
392 the NMR titration experiments and prediction of the interaction residues, were used to drive a
393 HADDOCK-docking simulation [31] as described under Materials and Methods. The top
394 scoring HADDOCK model from the highest scoring cluster was selected (HADDOCK Score

395 -107.8 ± -6.4 ; Restraint violation energy: 162.4 ± 50.16 Kcal/mol; Buried surface area:
396 $2,403.2 \pm 190.8$ Å; Z-score: -0.7). The resulting *EfAhpF*₃₅₄₋₅₆₀-*AhpC*₁₋₁₆₇ complex model
397 (Fig. 9) indicates the spatial proximity of the regions including the two catalytic cysteine
398 residues C493 and C496 in *EfAhpF*₃₅₄₋₅₆₀ with the *EfAhpC*₁₋₁₆₇ dimer. The *EfAhpC*₁₋₁₆₇ dimer
399 contacts this interface mainly with regions including the two helices $\alpha 2'$ of the 1st monomer
400 and $\alpha 6$ of the 2nd monomer (Fig. 9). Helix $\alpha 6$, followed by a loop (residues 161-167) region
401 holding C_R (C166), and $\alpha 2'$ helix holding C_P (C47) are linked to form a protein-protein
402 interaction scaffold, which fits into the groove on the binding surface of *EfAhpF*₃₅₄₋₅₆₀ (Fig.
403 9). Residues including G448-L455, S490-F495 comprise the major interaction cleft, forming
404 contact with the binding scaffold of the *EfAhpC*₁₋₁₆₇ dimer.

405

406 **4. Discussion**

407 **4.1 Unique features of the *E. faecalis* (V583) AhpR system**

408 Like the pathogenic *Mycobacterium tuberculosis*, vancomycin-resistant *E. faecalis* (V583)
409 represents a unique AhpR ensemble that evolved a variety of structural variations combined
410 with diverse mechanism to tackle stress caused by ROS. Unlike the well-studied *EcAhpC* and
411 *StAhpC*, which form a stable decamer in the reduced form and lower weight oligomers in the
412 oxidized state [8-10], the *Mycobacterial AhpC* (*MtbAhpC*) forms a dodecamer in a reduced
413 state [34,35], while *EfAhpC* forms a decamer independent to its redox state [7]. The gram-
414 negative *EcAhpC* and *StAhpC* contain two typical catalytic cysteine residues C_P and C_R [8-
415 10], while *MtbAhpC* harbours a third cysteine C176, proposed to reduce the disulphide
416 between C_P61 and C_R174 [34]. The gram-positive *EfAhpC* has two additional cysteines (C13,
417 C66), being relevant for stabilization of the decameric ring and enzyme activity [7].

418 The electron donor subunit of *EfAhpC*, *EfAhpF*, extends these variations for niche
419 adaptation by swapping of the usually N-terminal domain to the C-terminus (NTD_N/C

420 domain) and the CTD:Pyr_redox_2 domain to the N-terminus, a phenomenon discussed by
421 the concept of circular permutation, resulting in improved catalytic activity and altered
422 substrate or ligand binding affinity [36]. Despite the domain swapping, the linker connecting
423 the N- and C-terminal domains in *EfAhpF* is longer and more diverse in sequence compared
424 to its gram-negative counterparts [13]. Linker mutant studies demonstrated that the length of
425 the linker is required for optimal catalytic activity [13]. In addition, our recent *EfAhpF*- [13]
426 as well as the presented *EfAhpF* C503A mutant structure (Fig. 4) revealed the additional
427 ₄₀₉ILKDTEPAKELLYGIEKM₄₂₆-loop-helix stretch. Complete and partial deletion of this α 3-
428 helix affected protein stability and activity, respectively, identifying Y421 as a critical residue
429 [13]. The unique AhpF α 3-helix is proposed to interact with the C-terminus of AhpC, thereby
430 providing efficient electron transfer for AhpC for the final reduction of H₂O₂. Here, we
431 present for the first time that substitution of the extra C503 in *EfAhpF* increases the K_m for
432 AhpC ($70.9 \pm 12 \mu\text{M}$), resulting in a nearly 27-fold lower catalytic efficiency ($k_{cat}/K_m = 0.7 \times$
433 $10^5 \text{ M}^{-1}\cdot\text{s}^{-1}$ (Table. 2)). These data are in line with a significant reduction in H₂O₂
434 consumption, indicating the relevance of C503 in electron transfer from the electron donor
435 NADH via the electron centres of *EfAhpF* to the peroxidatic (C_p47) and resolving (C_R166')
436 cysteine residues in the catalytic centre of *EfAhpC*, where H₂O₂ is catalysed. Recently, we
437 showed, that substitution of the additional cysteine residues C13 and C66 affect *EfAhpC* ring
438 stabilization, which was directly related to a reduction of NADH-oxidation and H₂O₂
439 consumption [7]. The increasing reduction in H₂O₂ decomposition of the mutant ensemble
440 *EfAhpC* C66V-AhpF C503A followed by *EfAhpC* C13N-AhpF C503A and *EfAhpC*
441 C13N/C66-AhpF C503A, respectively (Fig. 3), confirms an additive effect and reflects that
442 these specific *EfAhpC*-AhpF cysteines are a prerequisite for proper ensemble formation and
443 maximum oxidation of its substrate NADH and the reduction of H₂O₂.

444

445 **4.2 Important residues of *EfAhpF*₃₅₄₋₅₆₀ for the redox process**

446 The NMR solution redox experiment of *EfAhpF*₃₅₄₋₅₆₀ sheds light into the residues of the
447 two-fold thioredoxin-like domain (NTD_N/C) which are affected by the process of electron
448 transfer (Fig. 5). The CSP analysis revealed that the residues W354, S428, G445, G449,
449 E451-N453, F488, C496, I499-C503, I506, H512, V518, V535, D641, and G533 undergo
450 significant alteration due to redox-dependent modulation (Fig. 5C-D). These residues do not
451 only include the extra cysteine C503 but also its close neighbourhood I499 to A502, and
452 I506, which together provide an area formed by the neighbouring helices α 4 and α 6 as well as
453 the β -sheets 5 and 6 (Fig. 5E). While the comparison of the atomic structures of WT- and
454 mutant *EfAhpF*₃₅₄₋₅₆₀ C503A nicely demonstrated that the C503 to A mutation does not alter
455 the secondary or tertiary structure of the protein, the NADH oxidation assay and NMR data
456 identify unequivocally its important role for the redox processes within *EfAhpF*₃₅₄₋₅₆₀.

457

458 **4.3 Critical binding epitope of *EfAhpF*₃₅₄₋₅₆₀ for assembling with *EfAhpC***

459 The electron transfer pathway after NADH oxidation in the pyridine nucleotide-disulfide
460 oxidoreductase domain (CTD:Pyr_redox_2) of *EfAhpF* is dictated by conformational changes
461 in the CTD:Pyr_redox_2 as well as by the movement of *EfAhpF*₃₁₄₋₅₆₀ relative to the
462 CTD:Pyr_redox_2 that enable the redox process between both disulfide centers (C134/C137
463 and C493/C496) [14,33]. The subsequent rearrangement of *EfAhpF*₃₅₄₋₅₆₀ to an extended form
464 of *EfAhpF* brings its disulfide center C493/C496 in proximity to the redox-active cysteines of
465 *EfAhpC*. The NMR titration experiment of full length *EfAhpC* and labelled *EfAhpF*₃₅₄₋₅₆₀
466 demonstrate that both *EfAhpR* subunits interact in a more dynamic and shorter-lived complex
467 (Fig. 6A-D). We recently predicted that the unravelled groove in the atomic structure of
468 *EfAhpF*₃₅₄₋₅₆₀ wrapping around the protein would provide an area for the packing of the C-
469 terminal tail of *EfAhpC* [13] as demonstrated for the *E. coli* AhpC [14]. While the C-terminus

470 of *EfAhpC* would bind to the backside of *EfAhpF*₃₅₄₋₅₆₀, the disulfide center C493/C496 of
471 *EfAhpF*₃₅₄₋₅₆₀ would come in neighbourhood to the catalytic disulphide (C_P47-C_R166) of
472 bound *EfAhpC*, and thereby providing rapid electron transfer. The titration and docking data
473 presented extend this prediction by identifying the amino acids G448-L455, S490-F495
474 comprising the major interaction cleft of *EfAhpF*₃₅₄₋₅₆₀. Interestingly, some of these sequence
475 segments were shown to be involved in the redox process within *EfAhpF*₃₅₄₋₅₆₀ as well. As
476 highlighted by the inset of figure 7C, residues within the proximity of residues V500, S502,
477 the additional C503, and I506, were found to undergo alterations during reduction of the
478 disulfide center C493/C496 of *EfAhpF*₃₅₄₋₅₆₀.

479 To summarize, our study proved the special role of the additional cysteine residue
480 (C503) present in the two-fold thioredoxin-like domain (NTD_N/C) of *EfAhpF* and that there
481 are alterations in its proximity during redox-state modulation. Moreover, we were able to
482 identify amino acid residues of *EfAhpF* involved in the interaction with its partner protein
483 *EfAhpC* and, therefore, to describe the mechanism of electron transfer from *EfAhpF* to
484 *EfAhpC* in detail. The data presented here enhance the knowledge of the key enzyme
485 complex AhpR important for ROS defense and ROS homeostasis. The knowledge of
486 systems' special features, the identification of species-specific structures, epitopes and
487 mechanisms, is an excellent basis for future drug development.

488

489 **Conflict of interest:** The authors declare that they have no conflicts of interest with the
490 contents of this article
491

492 **Author contributions**

493 YKT performed most of the experiments, analyzed the data and drafted the manuscript. JS
494 collected and analyzed the NMR data and drafted the manuscript. AMB collected and
495 analyzed the crystallography data and drafted the manuscript. NK collected and analyzed
496 stopped flow data and drafted the manuscript. AG purified labelled and unlabelled proteins
497 and helped editing of the manuscript. FE and BE helped perform the computational analysis
498 and editing of the manuscript. GG conceived the study and analyzed the data and wrote the
499 manuscript. All authors read and approved the manuscript.

500 **ACKNOWLEDGMENT**

501 This research was supported by a Singapore Ministry of Education Academic Research Fund
502 Tier 1 (RG140/16) to G.G. (M4080811.080). We thank Dr. S. S. M. Malathy for the art work
503 of Figure 1A.

504

505 **The abbreviations used are:** H₂O₂, hydrogen peroxide; AhpR, alkyl hydroperoxide
506 reductase; AhpF, alkyl hydroperoxide reductase subunit F; AhpC, alkyl hydroperoxide
507 reductase subunit C; C_P, peroxidatic cysteine; C_R, resolving cysteine; NADH, nicotinamide
508 adenine nucleotide; CTD:Pyr_redox_2, pyridine nucleotide-disulfide oxidoreductase domain;
509 NTD_N/C, thioredoxin-like domain; FAD, flavin adenine nucleotide; *EfAhpF*, *E. faecalis*
510 AhpF; TCEP, tris(2-carboxyethyl)phosphine

511

512 **References**

513 [1] C.A. Arias, B.E. Murray, The rise of the Enterococcus: beyond vancomycin resistance.

514 *Nature Rev. Microbiol.* 10 (2012) 266-278.

515 [2] M.A. Kohanski, D.J. Dwyer, B. Hayete, C.A. Lawrence, J.J. Collins, A common

516 mechanism of cellular death induced by bactericidal antibiotics. *Cell* 130 (2007) 797-810.

517 [3] M. Goswami, S.H. Mangoli, N. Jawali, Involvement of reactive oxygen species in the

518 action of ciprofloxacin against *Escherichia coli*. *Antimicrob. Agents Chemoth.* 50 (2006) 949-

519 954.

520 [4] J. Lu, A. Holmgren, The thioredoxin antioxidant system. *Free Rad. Biol. & Med.* 66

521 (2014) 75-87.

522 [5] X. Wang, X. Zhao, Contribution of oxidative damage to antimicrobial lethality.

523 *Antimicrob. Agents Chemoth.* 53 (2009) 1395-1402.

524 [6] Y. Arimura, T. Yano, M. Hirano, Y. Sakamoto, N. Egashira, R. Oishi, Mitochondrial

525 superoxide production contributes to vancomycin-induced renal tubular cell apoptosis. *Free*

526 *Rad. Biol. & Med.* 52 (2012) 1865-1873.

527 [7] A. Pan, A.M. Balakrishna, W. Nartey, A. Kohlmeier, P.V. Dip, S. Bhushan, G. Grüber,

528 Atomic Structure and enzymatic insights into the vancomycin-resistant *Enterococcus faecalis*

529 (V583) alkylhydroperoxide reductase subunit C. *Free Rad. Biol. & Med.* 115 (2018) 252-265.

530 [8] P.V. Dip, N. Kamariah, W. Nartey, C. Beushausen, V.A. Kostyuchenko, T.S. Ng, S.M.
531 Lok, W.G. Saw, F. Eisenhaber, B. Eisenhaber, G. Grüber, Key roles of the *Escherichia coli*
532 AhpC C-terminus in assembly and catalysis of alkylhydroperoxide reductase, an enzyme
533 essential for the alleviation of oxidative stress. *Biochim. Biophys. Acta – Bioenergetics* 1837
534 (2014) 1932-1943.

535 [9] P.V. Dip, N. Kamariah, M.S. Subramanian Manimekalai, W. Nartey, A.M. Balakrishna,
536 F. Eisenhaber, B. Eisenhaber, G. Grüber, Structure, mechanism and ensemble formation of
537 the alkylhydroperoxide reductase subunits AhpC and AhpF from *Escherichia coli*. *Acta*
538 *Crystallogr. D* 70 (2014) 2848-2862.

539 [10] Z.A. Wood, L.B. Poole, R.R. Hantgan, P.A. Karplus, Dimers to doughnuts: redox
540 sensitive oligomerization of 2-cysteine peroxiredoxins. *Biochemistry* 41 (2002) 5493-5504.

541 [11] A. Perkins, K.J. Nelson, D. Parsonage, L.B. Poole, P.A. Karplus, Peroxiredoxins:
542 guardians against oxidative stress and modulators of peroxide signalling. *TIBS* 40 (2015)
543 435-445.

544 [12] N. Kamariah, M.S. Manimekalai, W. Nartey, F. Eisenhaber, B. Eisenhaber, G. Grüber,
545 Crystallographic and solution studies of NAD(+)- and NADH-bound alkylhydroperoxide
546 reductase subunit F (AhpF) from *Escherichia coli* provide insight into sequential enzymatic
547 steps. *Biochim. Biophys. Acta – Bioenergetics* 1847 (2015) 1139-1152.

548 [13] Y.K. Toh, A.M. Balakrishna, M.S.S. Manimekalai, B.B. Chionh, R.R.C. Seetharaman,
549 F. Eisenhaber, B. Eisenhaber, G. Grüber, Novel insights into the vancomycin-resistant
550 *Enterococcus faecalis* (V583) alkylhydroperoxide reductase subunit F. *Biochim. Biophys.*
551 *Acta – Gen. Sub.* 1861 (2017) 3201-3214.

552 [14] W. Nartey, S. Basak, N. Kamariah, M.S. Manimekalai, S. Robson, G. Wagner, B.
553 Eisenhaber, F. Eisenhaber, G. Grüber, NMR studies reveal a novel grab and release

554 mechanism for efficient catalysis of the bacterial 2-Cys peroxiredoxin machinery. *FEBS J.*
555 282 (2015) 4620-4638.

556 [15] G. Grüber, J. Godovac-Zimmermann, T.A. Link, Ü. Coskun, V.F. Rizzo, C. Betz, S.M.
557 Bailer, Expression, purification, and characterization of subunit E, an essential subunit of the
558 vacuolar ATPase. *Biochem. Biophys. Res. Comm.* 298 (2002) 383-391.

559 [16] Z. Otwinowski, W. Minor, Processing of X-ray diffraction data collected in oscillation
560 mode. *Meth. Enzymol.* 276 (1997) 307-326.

561 [17] A.J. McCoy, R.W. Grosse-Kunstleve, P.D. Adams, M.D. Winn, L.C. Storoni, R.J. Read,
562 Phaser crystallographic software. *J. Applied Crystallogr.* 40 (2007) 658-674.

563 [18] P. Emsley, K. Cowtan, Coot: model-building tools for molecular graphics. *Acta*
564 *Crystallogr. D* 60 (2004) 2126-2132.

565 [19] G.N. Murshudov, A.A. Vagin, E.J. Dodson, Refinement of macromolecular structures by
566 the maximum-likelihood method. *Acta Crystallogr. D* 53 (1997) 240-255.

567 [20] V.B. Chen, W.B. Arendall, 3rd, J.J. Headd, D.A. Keedy, R.M. Immormino, G.J. Kapral,
568 L.W. Murray, J.S. Richardson, D.C. Richardson, MolProbity: all-atom structure validation
569 for macromolecular crystallography. *Acta Crystallogr. D* 66 (2010) 12-21.

570 [21] P.D. Adams, P.V. Afonine, G. Bunkoczi, V.B. Chen, I.W. Davis, N. Echols, J.J. Headd,
571 L.W. Hung, G.J. Kapral, R.W. Grosse-Kunstleve, A.J. McCoy, N.W. Moriarty, R. Oeffner,
572 R.J. Read, D.C. Richardson, J.S. Richardson, T.C. Terwilliger, P.H. Zwart, PHENIX: a
573 comprehensive Python-based system for macromolecular structure solution. *Acta Crystallogr.*
574 *D* 66 (2010) 213-221.

575 [22] W. DeLano, The *PyMOL* molecular Graphics System, DeLano Scientific, San Carlos,
576 CA, (2002).

577 [23] R. Maiti, G.H. Van Domselaar, H. Zhang, D.S. Wishart, SuperPose: a simple server for
578 sophisticated structural superposition. *Nucl. Acids Res.* 32 (2004) W590-594.

579 [24] M.D. Winn, An overview of the CCP4 project in protein crystallography: an example of
580 a collaborative project. *J. Synchr. Rad.* 10 (2003) 23-25.

581 [25] M.D. Winn, C.C. Ballard, K.D. Cowtan, E.J. Dodson, P. Emsley, P.R. Evans, R.M.
582 Keegan, E.B. Krissinel, A.G. Leslie, A. McCoy, S.J. McNicholas, G.N. Murshudov, N.S.
583 Pannu, E.A. Potterton, H.R. Powell, R.J. Read, A. Vagin, K.S. Wilson, Overview of the
584 CCP4 suite and current developments. *Acta Crystallogr. D* 67 (2011) 235-242.

585 [26] D. Rovnyak, D.P. Frueh, M. Sastry, Z.Y. Sun, A.S. Stern, J.C. Hoch & G. Wagner
586 Accelerated acquisition of high resolution triple-resonance spectra using non-uniform
587 sampling and maximum entropy reconstruction. *J. Magn. Res.* 170 (2004) 15-21.

588 [27] V.Y. Orekhov, V.A. Jaravine (2011) Analysis of non-uniformly sampled spectra with
589 multi-dimensional decomposition. *Prog. Nucl. Magn. Reson. Spectrosc.* **59**, 271-292.

590 [28] K. Kazimierczuk, V.Y. Orekhov (2010) Accelerated NMR Spectroscopy by using
591 compressed Sensing. *Angew. Chem.-Int. Edit.* **50**, 5556-5559.

592 [29] F. Delaglio, S. Grzesiek, G.W. Vuister, G. Zhu, J. Pfeifer, A. Bax, NMRPipe: a
593 multidimensional spectral processing system based on the UNIX pipes. *J. Biomol. NMR.* 6
594 (1995) 277-293.

595 [30] T.D. Goddard, D.G. Kneller, SPARKY, version 3 (2007), University of California, San
596 Francisco, CA.

597 [31] S.J. de Vries, M. van Dijk, A.M. Bonvin (2010) The HADDOCK web server for data-
598 driven biomolecular docking. *Nature Prot.* 5 (2010), 883–897.

599 [32] S.B. Qin, H.X. Zhou, meta-PPISP: a meta web server for protein-protein interaction site
600 prediction. *Bioinformatics* 23 (2007), 3386-3387.

601 [33] L.B. Poole, A. Godzik, A. Nayeem, J.D. Schmitt, AhpF can be dissected into two
602 functional units: tandem repeats of two thioredoxin-like folds in the N-terminus mediate

603 electron transfer from the thioredoxin reductase-like C-terminus to AhpC. *Biochemistry* 39
604 (2000) 6602-6615.

605 [34] B.G. Guimaraes, H. Souchon, N. Honore, B. Saint-Joanis, R. Brosch, W. Shepard, S.T.
606 Cole, P.M. Alzari, Structure and mechanism of the alkyl hydroperoxidase AhpC, a key
607 element of the *Mycobacterium tuberculosis* defense system against oxidative stress. *J. Biol.*
608 *Chem.* 280 (2005) 25735-25742.

609 [35] C.F. Wong, J. Shin, M.S. Subramanian Manimekalai, W.G. Saw, Z. Yin, S. Bhushan, A.
610 Kumar, P. Raguathan, G. Grüber, AhpC of the mycobacterial antioxidant defense system
611 and its interaction with its reducing partner Thioredoxin-C. *Sci. Rep.* 7 (2017) 5159.

612 [36] Y. Yu, S. Lutz, Circular permutation: a different way to engineer enzyme structure and
613 function. *Trends Biotechnol.* 29 (2011) 18-25.

614 [37] C. Notredame, D.G. Higgins, J. Heringa, T-Coffee: A Novel Method for Fast and
615 Accurate Multiple Sequence Alignment. *J. Mol. Biol.* 302 (2000) 205-217.

616 [38] A.M. Waterhouse, J.B. Procter D.M.A. Martin, M. Clamp, G.J. Barton, Jalview
617 Version 2 – a multiple sequence alignment editor and analysis workbench. *Bioinformatics* 25
618 (2009) 1189-1191.

619

620

621

622

623

624

625

626

627 **Table 1:** Data collection and refinement statistics

Wavelength (Å)	1.00
Space group	P4 ₁ 32
Unit cell parameters (Å)	$a = b = c = 134.101$ $\alpha = \beta = \gamma = 90^\circ$
Resolution range (Å)	30-2.5
Solvent content (%)	72.06
Total number of reflections	166,667
Number of unique reflections	14,035
$I/\sigma(I)^a$	22.4 (7.3)
Completeness (%)	99.7 (99.7)
R_{merge}^b (%)	6.9 (25.2)
Redundancy	11.2 (11.7)

628

Refinement Statistics

R factor ^c (%)	21.47
R free ^d (%)	26.72

Number of amino acid residues	207
-------------------------------	-----

Ramachandran statistics

Favored (%)	98.1
Generously (%)	1.9
Disallowed (%)	0.0

R.M.S. Deviations

Bond lengths (Å)	0.006
Bond angles (°)	1.088

Mean atomic B values

Overall	61.02
Wilson B Factor	48.63

CC1/2	99.9 (97.5)
CC*	100 (99.4)

Clash score	1.22
Molprobity score:	1.23

629

630 ^a Values in parentheses refer to the corresponding values of the highest resolution shell (2.59 – 2.5 Å).631 ^b $R_{\text{merge}} = \sum_i |I_h - I_{hi}| / \sum_i I_h$, where I_h is the mean intensity for reflection h .632 ^c R-factor = $\sum |F_o| - |F_c| / \sum |F_o|$, where F_o and F_c are measured and calculated structure factors, respectively.633 ^d R-free = $\sum |F_o| - |F_c| / \sum |F_o|$, calculated from 5% of the reflections selected randomly and omitted during refinement.

634

635 **Table 2:** Kinetic constants for WT *EfAhpF* and mutant *EfAhpF* C503A.

<i>EfAhpF</i>	k_{cat} (s ⁻¹)	K_m (AhpC) (μM)	k_{cat}/K_m (AhpC) (M ⁻¹ ·s ⁻¹)
WT	46.1 ± 4	24.5 ± 5	1.9 × 10 ⁶
C503A	49.2 ± 6	70.9 ± 12	0.7 × 10 ⁵

636

637 **Figure Legends**

638 **Figure 1.** The proposed catalytic cycle of the *EfAhpC*-AhpF ensemble and multiple sequence
639 alignment of the NTD_N/C domain of subunit AhpF. (A) *EfAhpC* exists as a decameric ring
640 in both oxidized and reduced states [7]. In the crystal structure of the reduced *EfAhpC*₁₋₁₇₂
641 [7], the C_p loop exists in two different conformations as shown in the *inset boxes*. In the
642 reduced state of *EfAhpC* the peroxidative cysteine C_p in the fully folded (FF) conformation
643 attacks H₂O₂ and reduces it to H₂O. In this process, C_p is converted into sulfenic acid (C_p-
644 SOH form). The resolving cysteine, C_R, then attacks the C_p-SOH form to generate an inter-
645 molecular disulphide bond. Subsequently, this disulphide bonded form of C_p undergoes a
646 conformational change to a locally unfolded form (LU). This disulphide is then resolved by
647 the interacting partner, AhpF. The recently determined low resolution solution structure of
648 the dimeric *EfAhpF* with the crystal structure of *EfAhpF*₃₅₄₋₅₆₀ [13] inside. The unique loop in
649 *EfAhpF*₃₅₄₋₅₆₀ with the short helix ₄₀₉ILKDTEPAKELLYGIEKM₄₂₆ is marked with an
650 asterisk. (B) Multiple sequence alignment of the NTD_N/C domain of subunit AhpF from ten
651 different species was performed using T-coffee algorithm [37] embedded within Jalview
652 program [38]. The secondary structure elements of *EfAhpF*₃₅₄₋₅₆₀ are shown above the
653 sequence. Conserved residues are highlighted in *blue*. The CXXC conserved motif is outlined
654 in *green* box. *EfAhpF* C503 and its equivalent residues from other species are outlined in *red*
655 box.

656

657 **Figure 2.** Enzymatic characterization of WT *EfAhpF* and its mutant. Michaelis-Menten plot
658 of 0.5 – 40 μM of *EfAhpC* WT with 50 nM of (A) *EfAhpF* WT or (B) *EfAhpF* C503A. Data
659 shown are mean of triplicates.

660

661 **Figure 3.** FOX assay of WT *EfAhpF* (*brown*) and *EfAhpF* C503A (*blue*) with *EfAhpC* (*A*).
662 Data shown are mean of triplicates. (*B*) FOX assay data of *EfAhpF* C503A with WT *EfAhpC*
663 (*brown*), *EfAhpC* C13N (*red*), C66V (*green*) and double-mutant C13N/C66V (*blue*). Data
664 shown are mean of triplicates.

665

666 **Figure 4.** Cartoon representation of one monomer of the *EfAhpF*₃₅₄₋₅₆₀ C503A mutant
667 structure shown in *pale green*, the α -helices and β -strands are labelled (*A*). Catalytic site
668 cysteines 493 and 496 including the disulfide bond are shown in *yellow* spheres. The C503A
669 mutation is shown in *red* spheres. (*B*) *EfAhpF*₃₅₄₋₅₆₀ C503A, *pale green* is overlapped with
670 WT *EfAhpF*₃₅₄₋₅₆₀, *blue* (PDB ID: 5H29). Catalytic site cysteines 493 and 496, including the
671 disulfide bond, are shown in *yellow* spheres. C503A mutation is shown in *red* spheres.

672

673 **Figure 5.** NMR spectroscopic characterization of *EfAhpF*₃₁₄₋₅₆₀. (*A*) ¹⁵N-¹H TROSY-HSQC-
674 spectrum of *EfAhpF*₃₅₄₋₅₆₀. The spectrum was recorded at 298K on a Bruker Avance 700
675 MHz spectrometer. The assignments for resolved backbone residues are labelled with in letter
676 amino acid code and residue number. (*B*) The secondary structural elements crystal structure
677 of *EfAhpF*₃₅₄₋₅₆₀ from the experimentally determined crystal structure. The scores were
678 calculated from $\Delta C\alpha$ values based on backbone assignment of *EfAhpF*₃₅₄₋₅₆₀. Contiguous
679 positive and negative chemical shift index values correspond to α -helices and β -strands,
680 respectively. (*C*) Selected sections of some *EfAhpF*₃₅₄₋₅₆₀ residues showing cross-peaks and
681 undergoing significant changes of chemical shifts during redox modulation. (*D*) Chemical
682 shift perturbation (CSP) analysis between reduced and oxidized *EfAhpF*₃₅₄₋₅₆₀. Weighted
683 CSPs for the ¹⁵N and ¹H resonance of reduced and oxidized *EfAhpF*₃₅₄₋₅₆₀ residues revealing
684 CSP above 0.1 ppm (*solid line*) are labeled as one-letter code. The weighted CSPs between
685 reduced and oxidized *EfAhpF*₃₅₄₋₅₆₀ for backbone ¹⁵N and ¹HN were calculated by the

686 formula $\Delta\delta = [(\Delta N/5)^2 + (\Delta HN)^2]^{0.5}$. The average weighted CSP(Avg) and Avg+standard
687 deviation(delta) values were displayed by dashed lines, respectively. (E) (top) Surface
688 representation of *EfAhpF*₃₅₄₋₅₆₀ displaying residues showing significant (CSP>0.1, red) and
689 moderate (0.05<CSP<0.1, green) CSP. (bottom) Ribbon representation of CSP analysis. The
690 region which undergoes significant CSP is marked as circle. Amino acid C503, which is
691 located in this region, is shown by stick representation and indicated by a line.

692

693 **Figure 6.** Interaction of *EfAhpC* with *EfAhpF*₃₅₄₋₅₆₀ as studied by NMR. (A) Summary of
694 gradual disappearance and decrease of intensities of the *EcAhpF*₃₅₄₋₅₆₀ cross-peaks in the
695 presence of increasing amount of its larger binding partner. A molar ratio of *EfAhpF*₃₅₄₋₅₆₀ to
696 *EfAhpC* of 1:0 (left), 1:0.05 (middle), and 1:0.1 (right) were used. (B) Selected sections for
697 some residues show cross-peaks which undergo significant decrease of peak intensities after
698 addition of *EfAhpC*.

699

700 **Figure 7.** NMR analysis of *EfAhpF*₃₅₄₋₅₆₀ and *EfAhpC*. The residues of flexible linker regions
701 were excluded from the analysis. (A) A plot of changes of peak intensity based on the ratio
702 (I_0/I_1) at a molar ratio of 1:0.1. The average value of the intensity ratio and standard deviation
703 were shown as dotted line and solid box, respectively. The residues showing higher intensity
704 ratio than standard deviation are labelled (B) Changes of ¹⁵N linewidth between the ¹H-¹⁵N
705 TROSY-HSQC resonances of *EfAhpF*₃₅₄₋₅₆₀ alone and in the presence of *EfAhpC* at a molar
706 ratio 1:0.1. The average value of the linewidth changes (ΔL) and standard deviation were
707 shown as dotted line and solid box, respectively. (C) Surface representation of *EfAhpF*₃₅₄₋₅₆₀
708 displaying residues showing significant and moderate decreased intensities (cyan and green
709 cyan), and residues showing significant (over than standard deviation) and moderate (over

710 than average) increase of linewidths (*green and light green*). The cysteine catalytic site of
711 *EfAhpF*₃₁₄₋₅₆₀ is shown in *red*.

712

713 **Figure 8.** NMR analysis of mutant *EfAhpF*₃₅₄₋₅₆₀ C503A. (A) CSP analysis of WT and *mutant*
714 *EfAhpF*₃₅₄₋₅₆₀ C503A. Calculation of weighted CSPs and analysis for the ¹⁵N- and ¹H
715 resonance of WT and *EfAhpF*₃₅₄₋₅₆₀ C503A were performed as described above. The average
716 weighted CSP(Avg) and Avg+standard deviation(delta) values were displayed by dashed
717 lines. Residues over than standard deviations are labelled as one letter code. (B) A plot of
718 changes of peak intensity based on the ratio (I_0/I_I) at a molar ratio of 1:0.1. The average
719 value of the intensity ratio and standard deviation were shown as dotted line and solid box,
720 respectively. The residues showing higher intensity ratios than standard deviation are
721 labelled. (C) Changes of ¹⁵N linewidth between the ¹H-¹⁵N TROSY-HSQC resonances of
722 *EfAhpF*₃₅₄₋₅₆₀ C503A alone and in the presence of *EfAhpC* at a molar ratio 1:0.1. The average
723 value of the linewidth changes (ΔL) and standard deviation were revealed as dotted line and
724 solid box, respectively.

725

726 **Figure 9.** The best result of HADDOCK docking displaying the *EfAhpF*₃₅₄₋₅₆₀-*AhpC*₁₋₁₆₇
727 ensemble. (A) Surface and ribbon representation of the *EfAhpF*₃₅₄₋₅₆₀-*AhpC*₁₋₁₆₇ complex.
728 The major binding contacts of the *EfAhpC*₁₋₁₆₇ dimer unit, including helical segment $\alpha 2'$ (1st
729 monomer) and $\alpha 6$ (2nd monomer) are labelled and displayed as *blue*. The catalytic C47 and
730 C166 of *EfAhpC*₁₋₁₆₇ are presented as sphere model. (B) The complex tilted at 30°. (C)
731 Extended section of the complex highlighting the catalytic residues C493 (*red*, *EfAhpF*₃₅₄₋₃₆₀)
732 and C47 (1st monomer of *EfAhpC*₁₋₁₆₇).

733

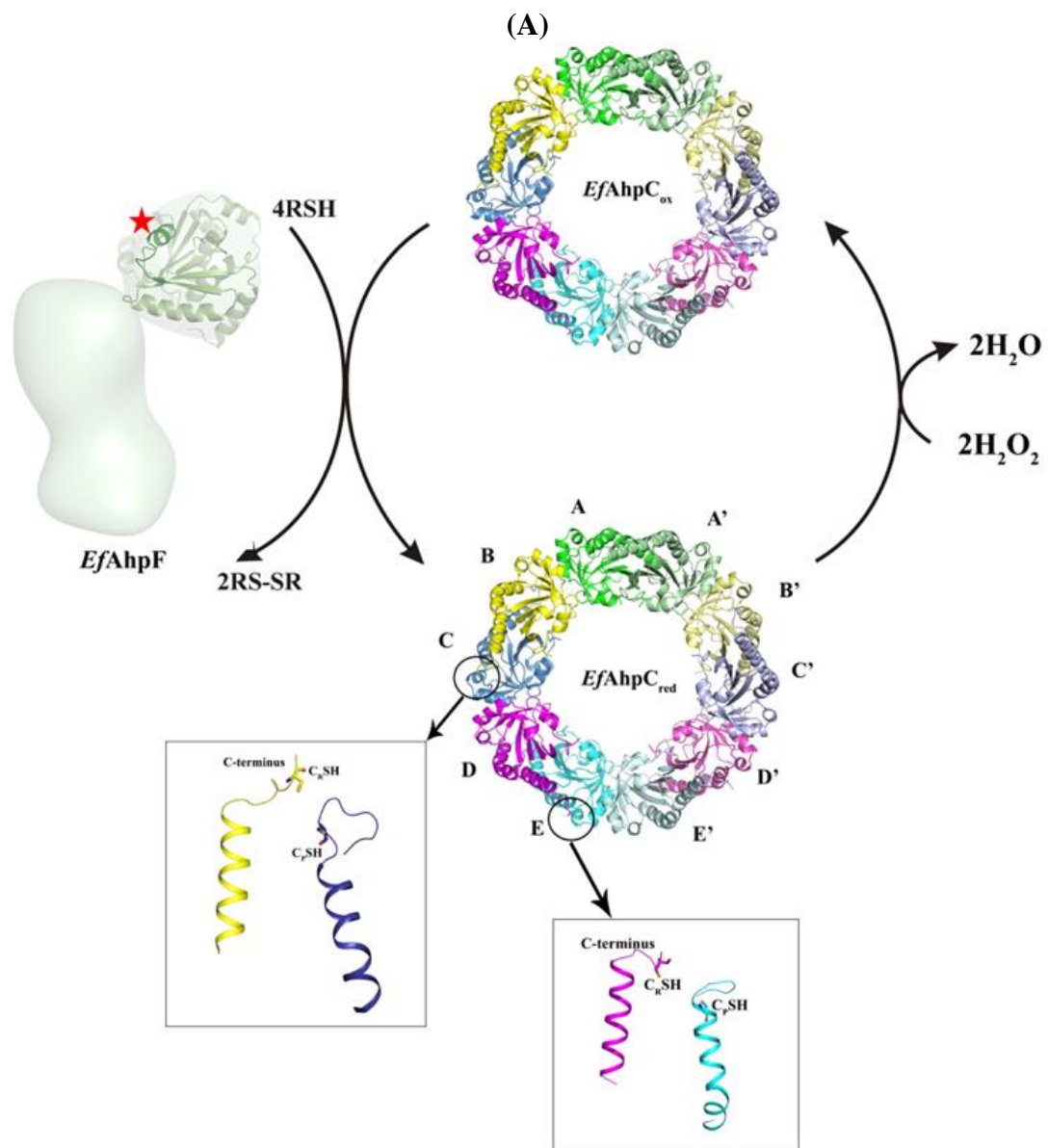


Figure 1A

(B)

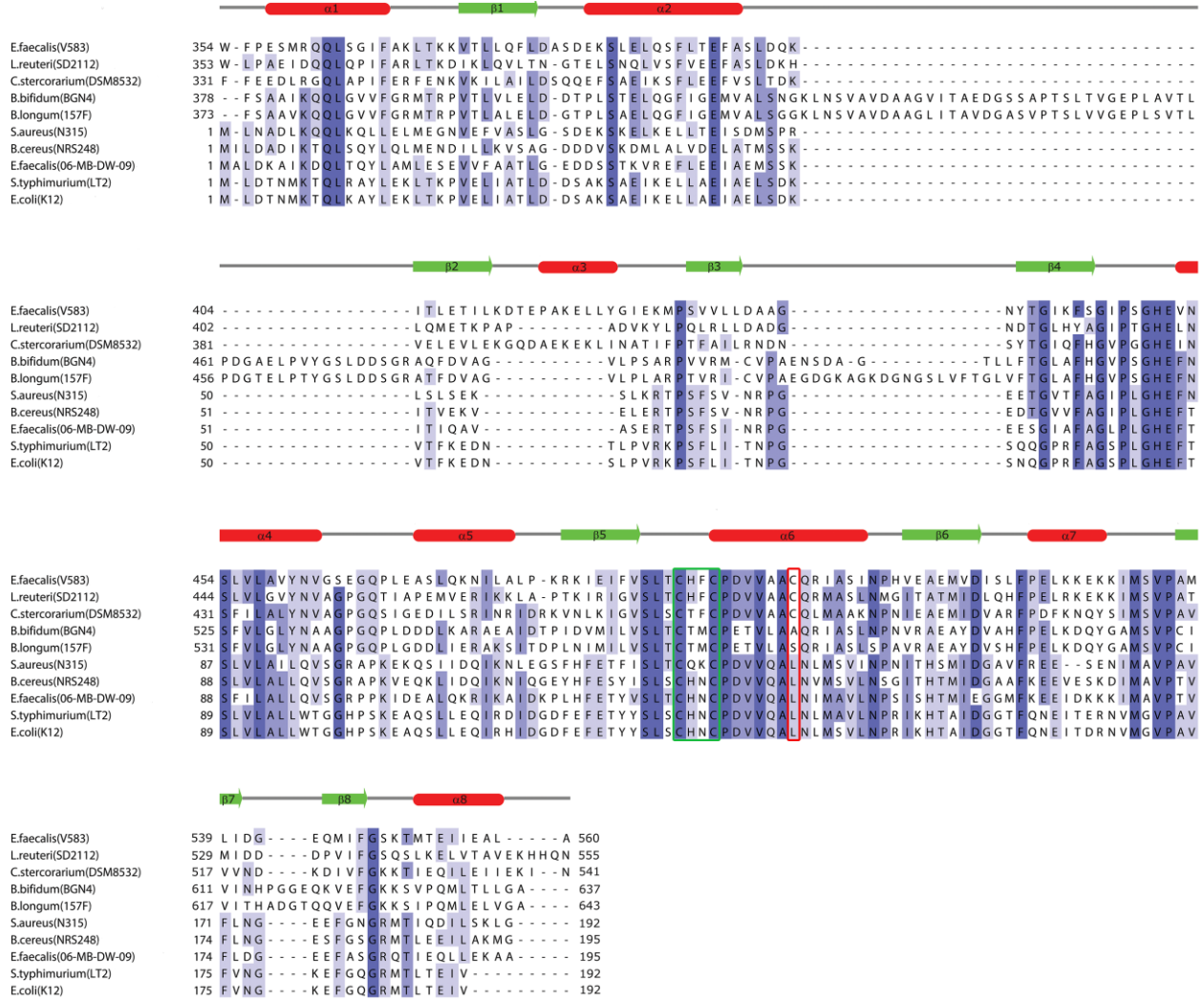
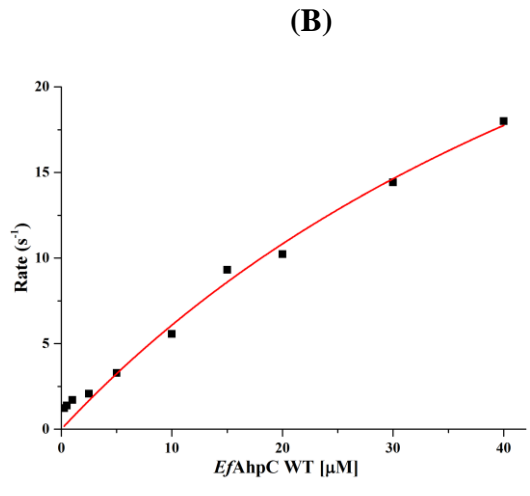
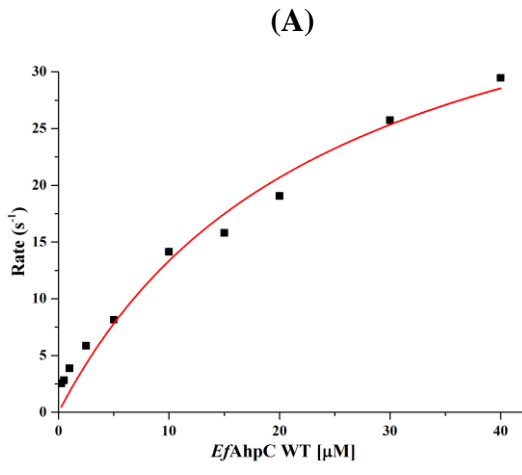
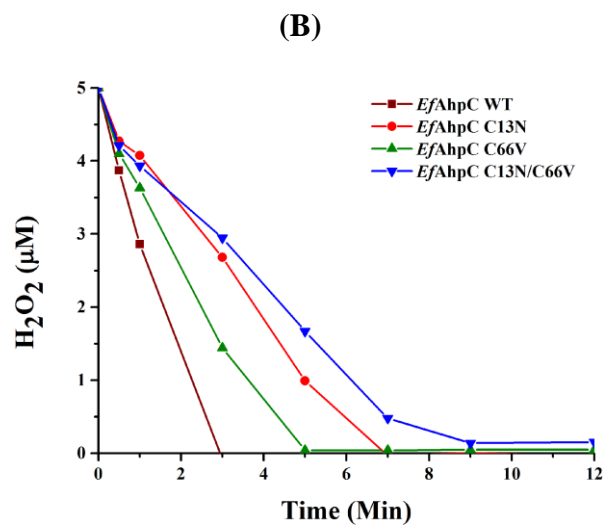
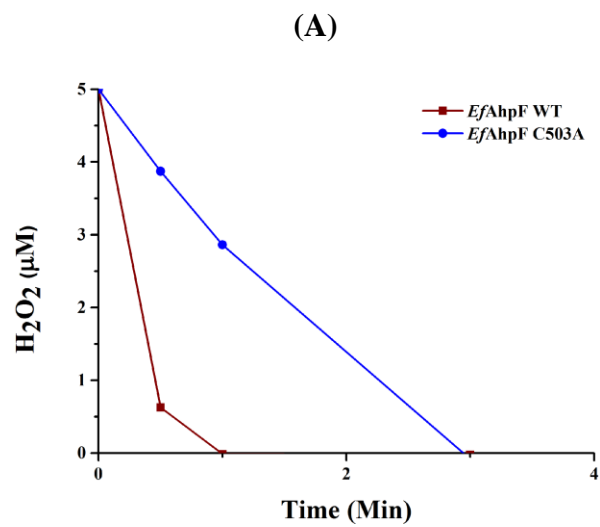


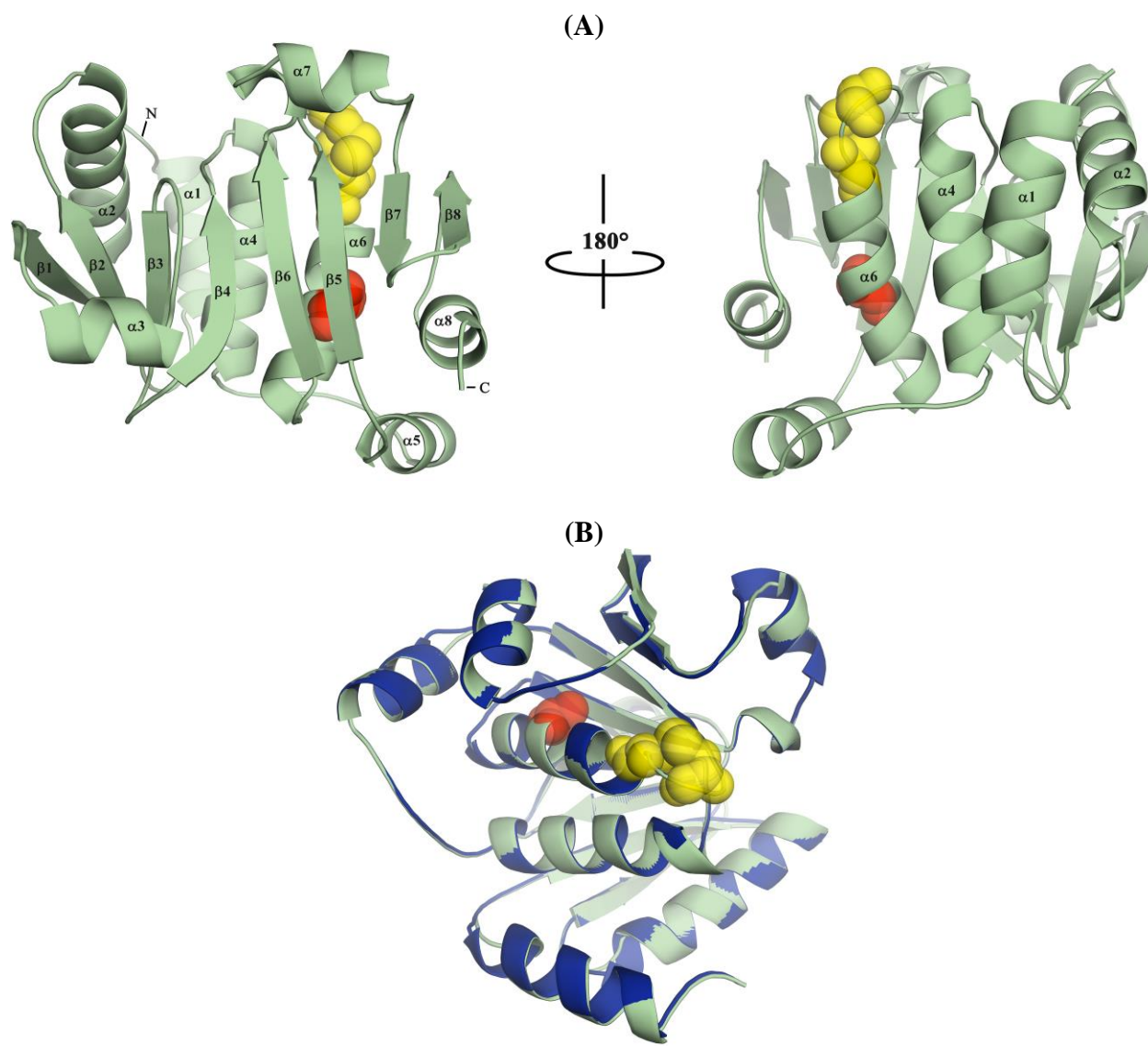
Figure 1B



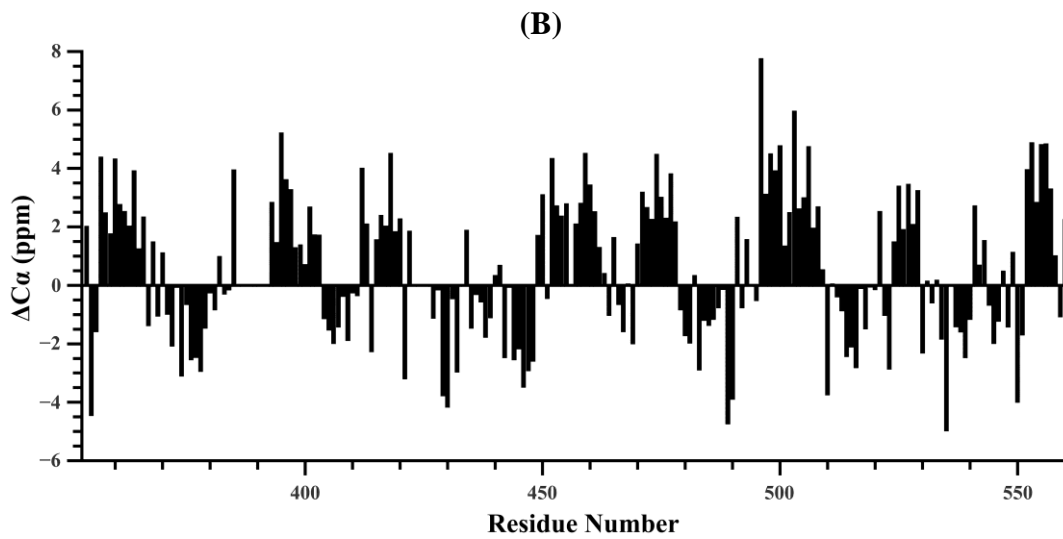
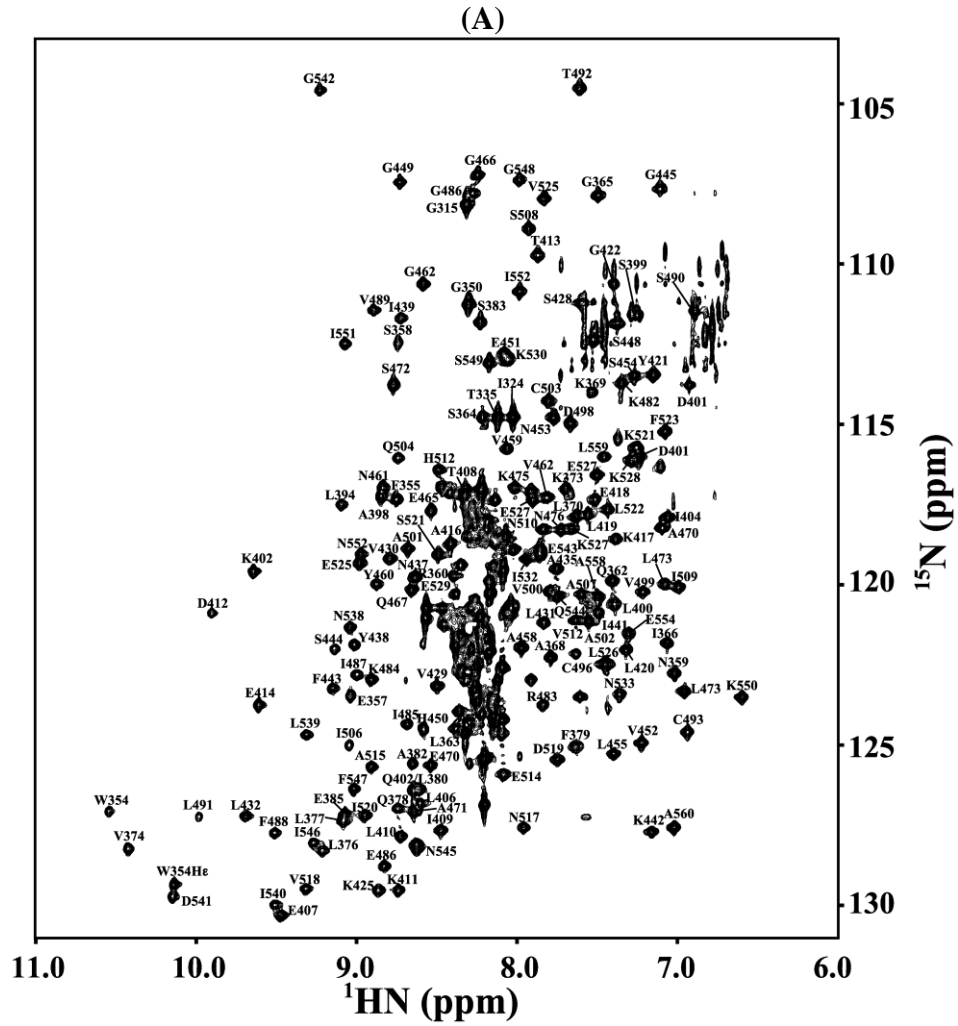
Figures 2A-B



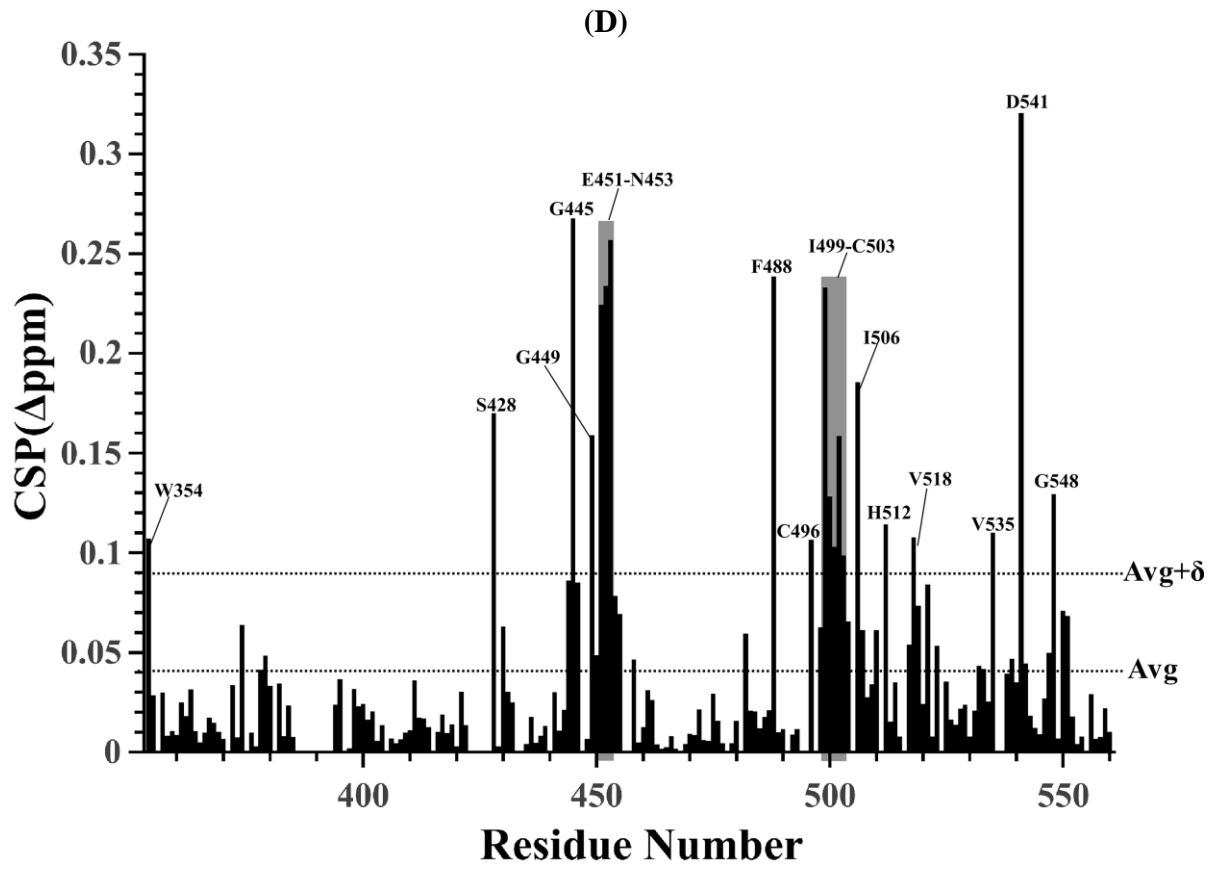
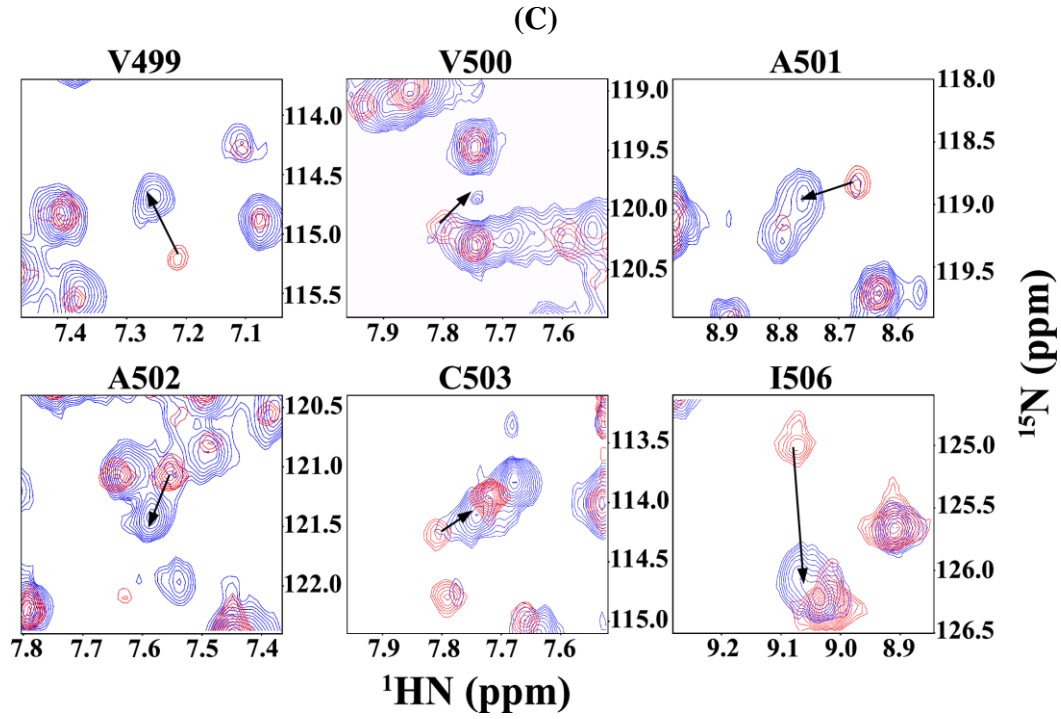
Figures 3A-B



Figures 4A-B



Figures 5A-B



Figures 5C-D

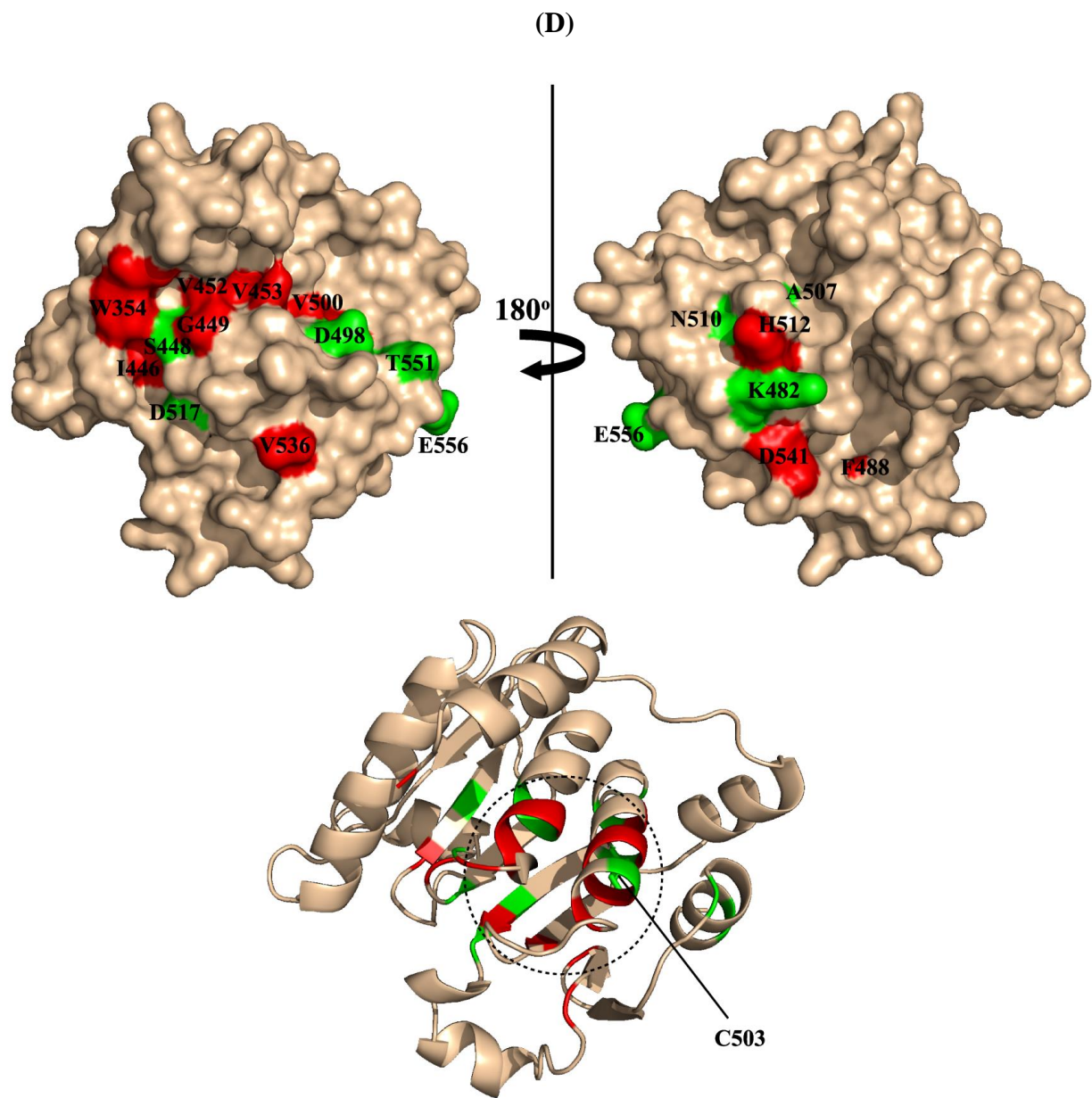
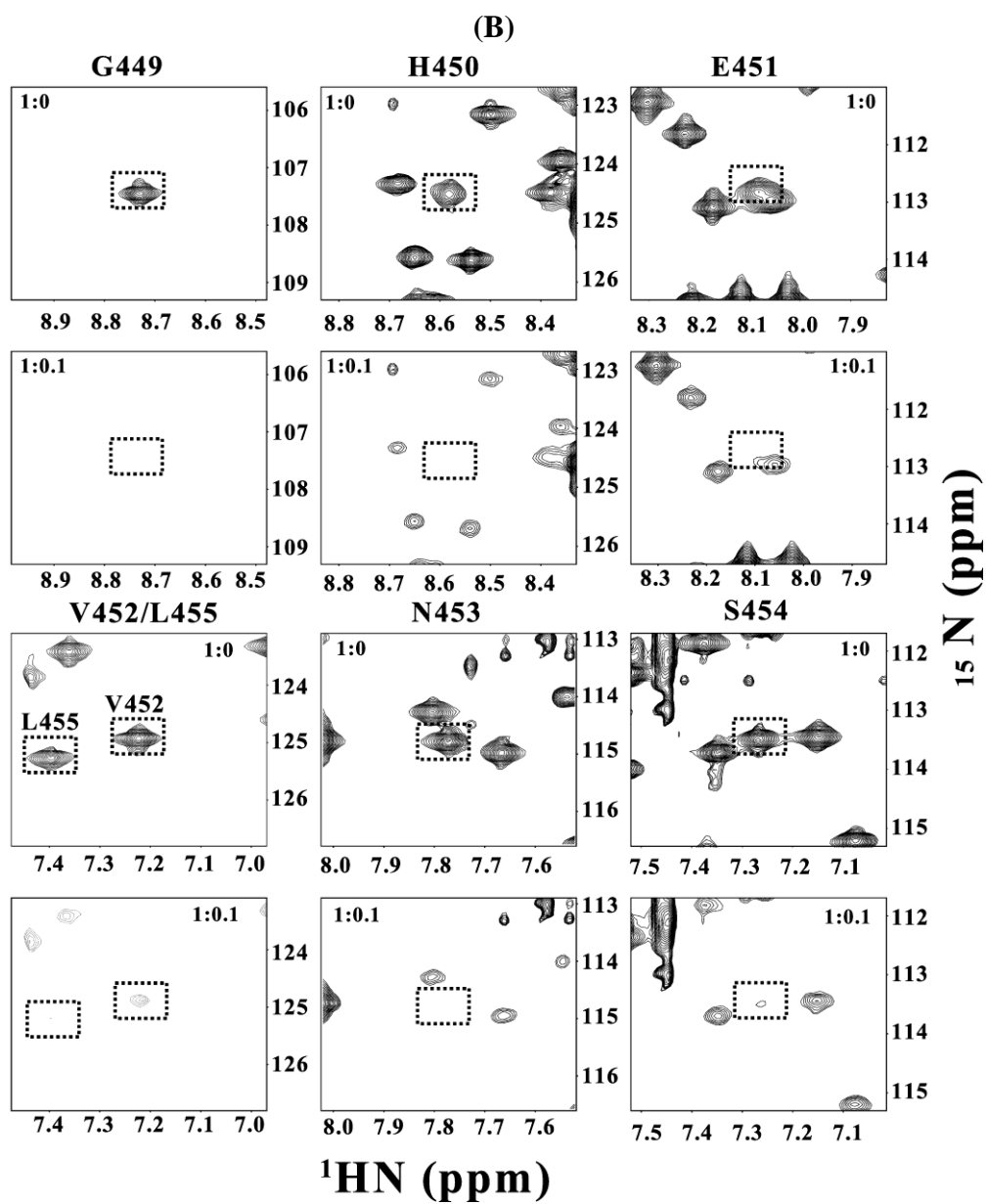
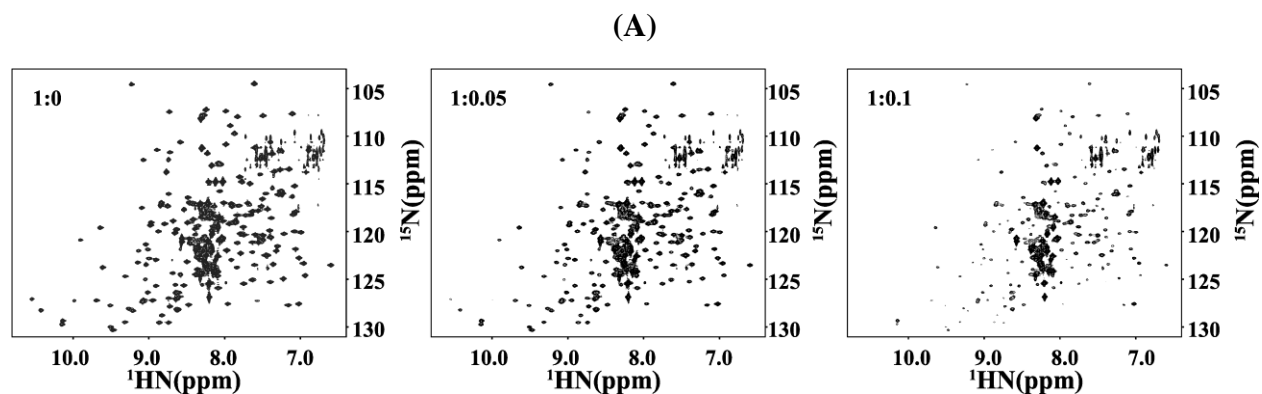
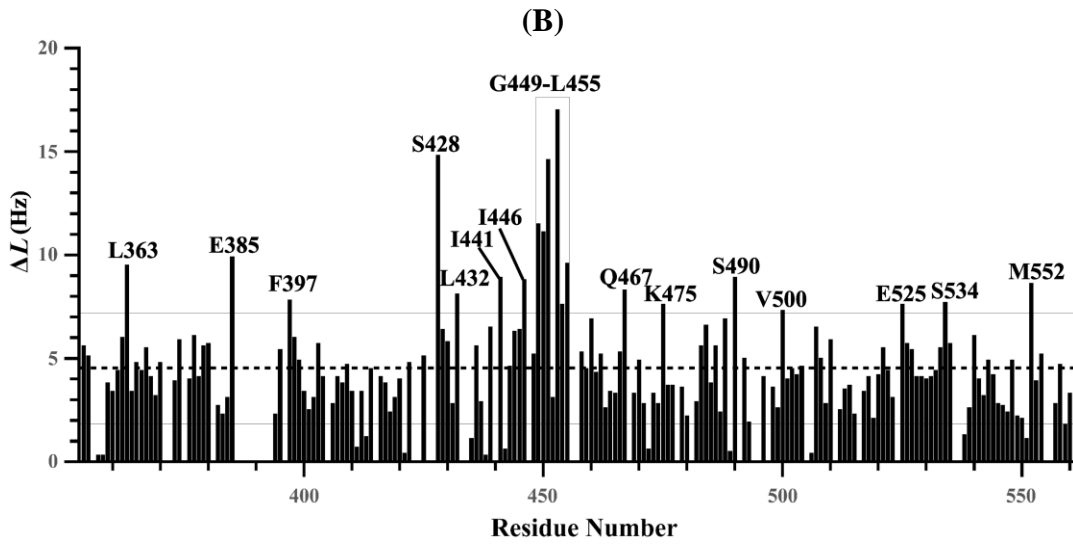
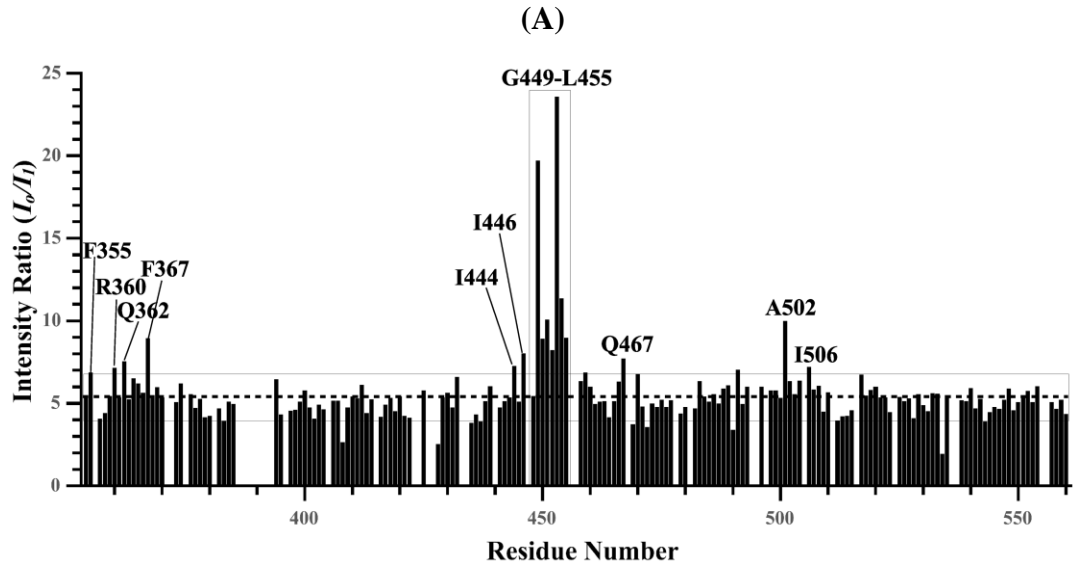


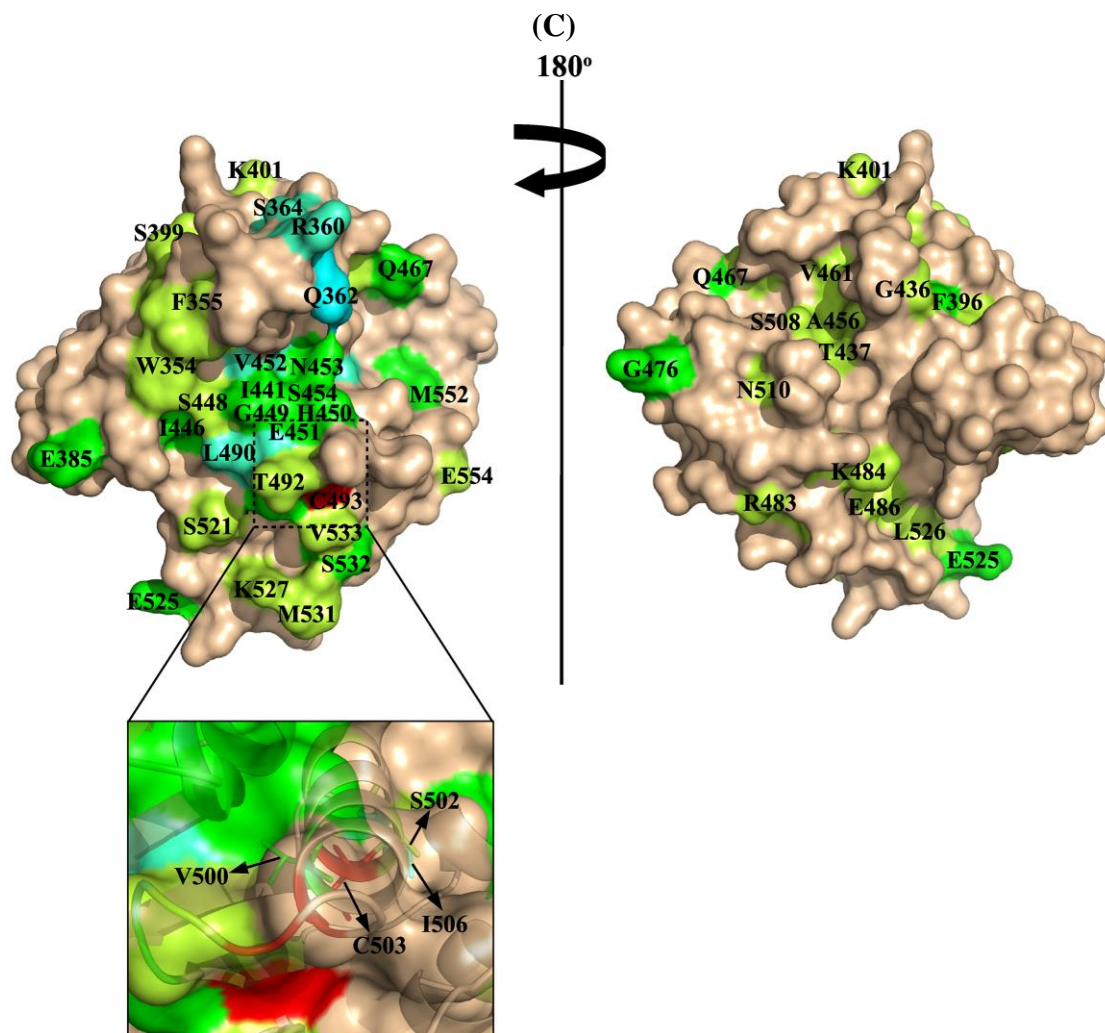
Figure 5E



Figures 6A-B



Figures 7A-B



Figures 7C

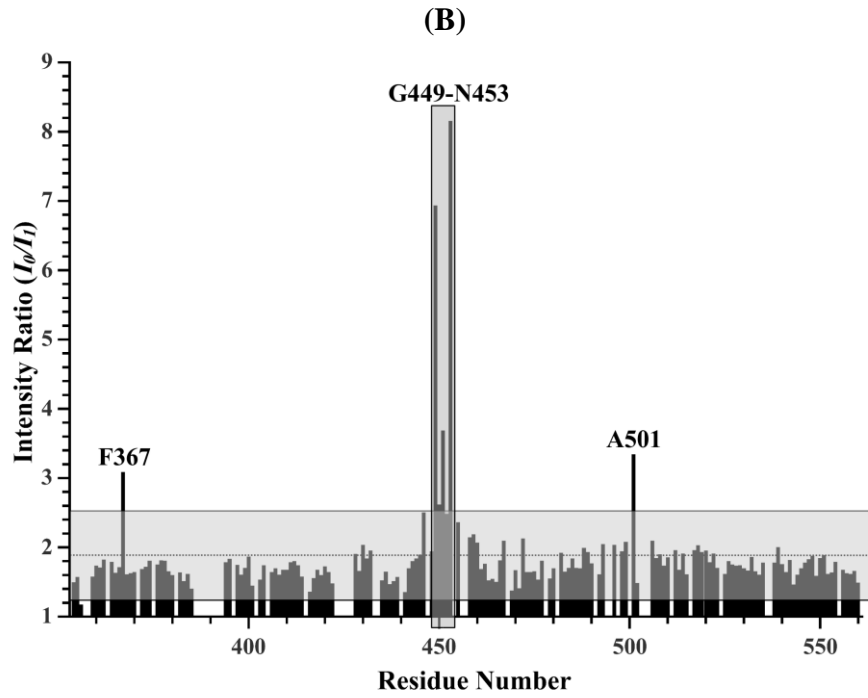
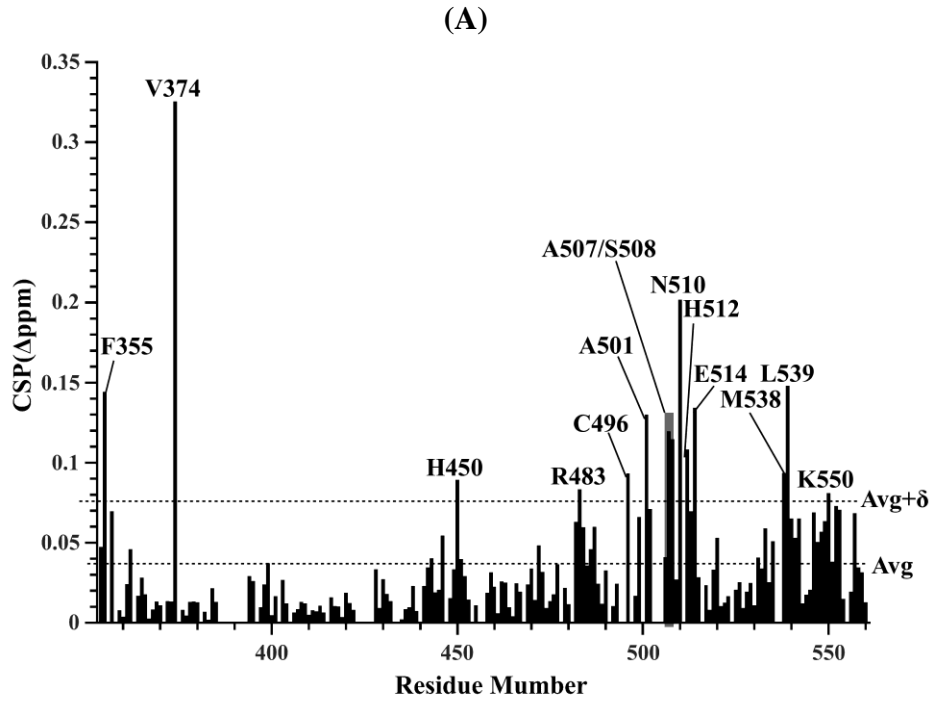


Figure 8A-B

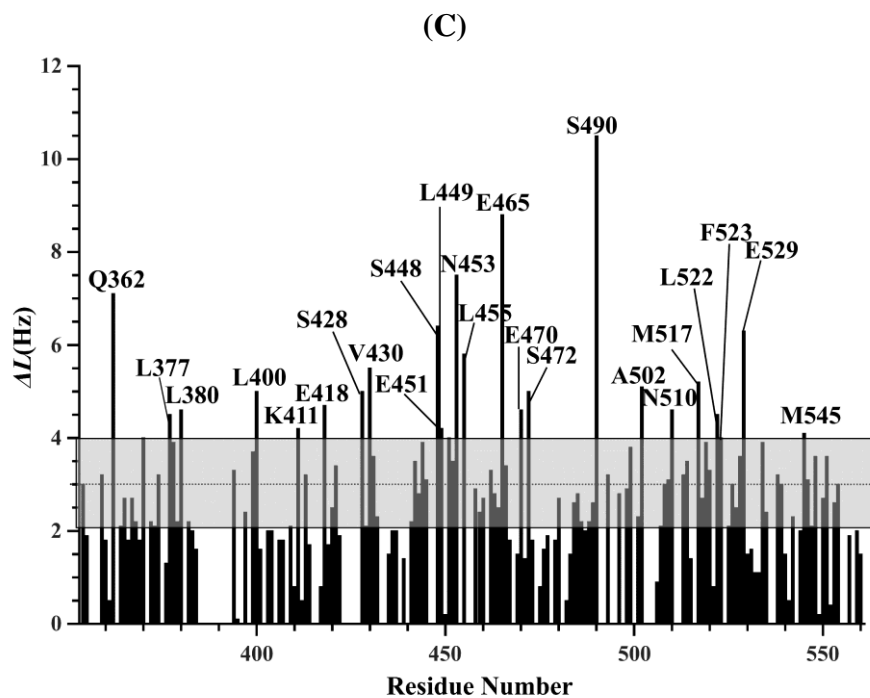


Figure 8C

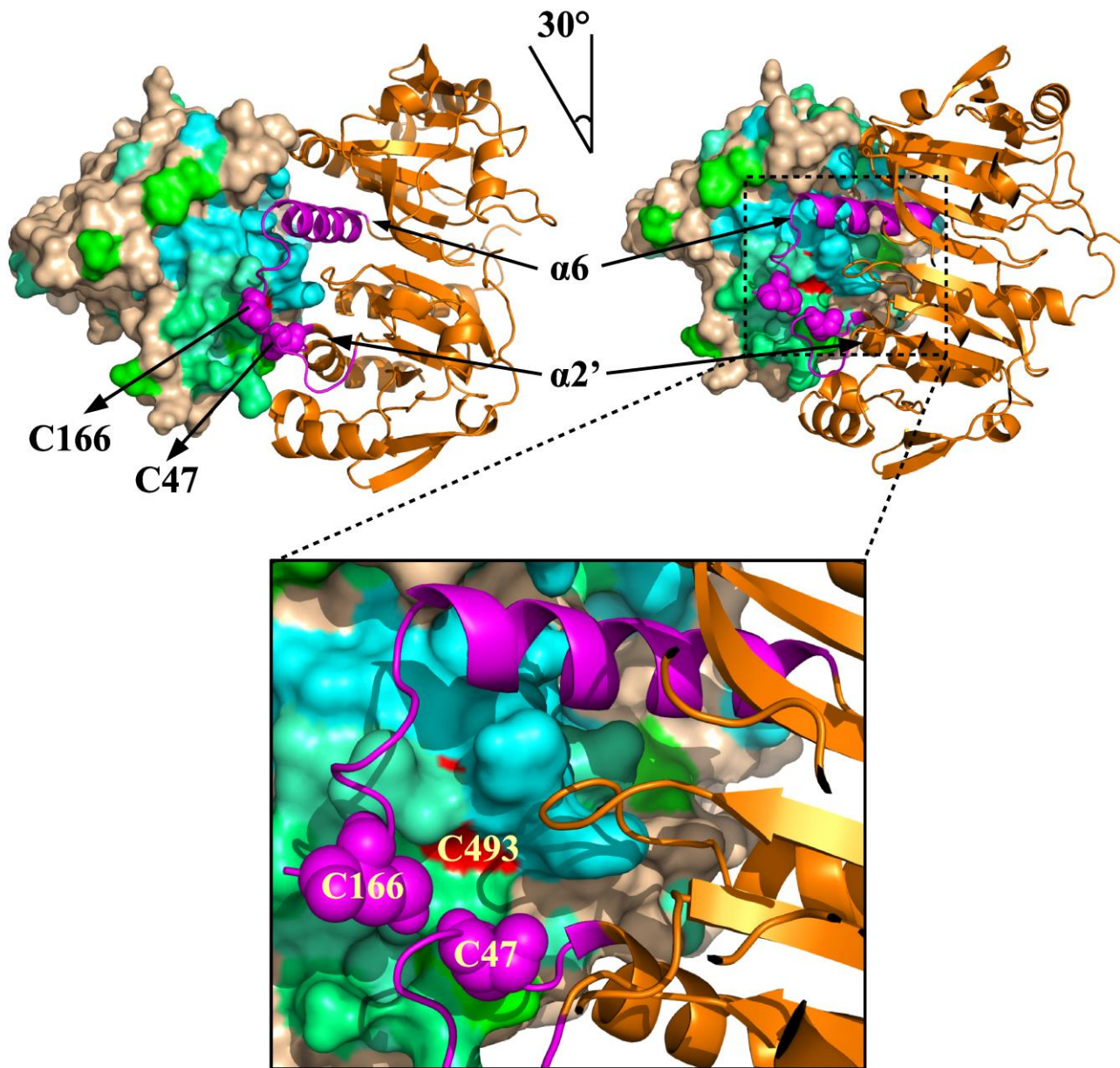


Figure 9